Thermal Spray Coating of Polymeric Composite Materials for De-icing and Anti-icing Applications

Alireza Rahimi

A Thesis

In the Department

of

Mechanical Industrial and Aerospace Engineering

Presented in Partial Fulfillment of the Requirements

for the Degree of

Master of Applied Science (Mechanical Engineering)

at Concordia University

Montreal, Quebec, Canada

August 2019

CONCORDIA UNIVERSITY

School of Graduate Studies

This is to certify that the thesis prepared

By: Alireza Rahimi

Entitled: Thermal Spray Coating of Polymeric Composite Materials for De-icing And Anti-icing Applications

and submitted in partial fulfillment of the requirements for the degree of

Master of Applied Science

complies with the regulations of the university and meets the accepted standards with respect to originality and quality.

Signed by the final Examining Committee:

_____ Chair
Dr. Daria Terekhov

_____ Internal Examiner
Dr. Carole El Ayoubi

_____ External Examiner
Dr. Ahmed Soliman

_____ Supervisor
Dr. Ali Dolatabadi

_____ Supervisor
Dr. Mehdi Hojjati

_____ Supervisor
Dr. Christian Moreau

Approved by _____
Chair of Department or Graduate Program Director

August 2019

_____
Dean, Gina Cody School of Engineering and Computer Science

ABSTRACT

Thermal Spray Coating of Polymeric Composite Materials for De-icing and Anti-icing Applications

Alireza Rahimi

Proper removal of accreted ice from the structures that are usually in contact with the harsh and cold weathers has always been a big challenge for the industry. Different methods and technologies have been adopted for ice management in wind turbines and aircraft. The purpose of this thesis is the fabrication of an electro-thermal heating element, as de-icer or anti-icer, for polymer-based composites. In this study, the plasma spray technique was utilized for the deposition of a nickel-chrome-aluminum-yttrium (NiCrAlY) coating layer as a heating element on top of a glass fiber-reinforced polymer composite (GFRP). For the fabrication of a high-quality and appropriate heating element coating layer, three types of composite samples with different surface types were manufactured. The first composite type was fabricated by the stacking of 16 GFRP prepregs, the second type was fabricated by the stacking of 16 GFRP and a 200 stainless steel mesh cloth as the top layer, and the last composite type was fabricated by the stacking 16 GFRP prepregs and a 400 stainless steel mesh cloth as the top layer. Moreover, to find the NiCrAlY powder with the proper particle size distribution for the generation of a heating element, two types of NiCrAlY powder with the fine and coarse particle size distributions were used for the coating of the composite samples. After coating of the composite samples with different spray parameters, and examining them under an optical microscope, it was found that using a 200 stainless steel mesh as the top layer of the composites makes a significant improvement in the uniformity, adhesion, deposition efficiency, and quality of the coatings. For more analysis, several tests were conducted on the coated samples for determining their mechanical and electrical properties. It was found that using a proper surface modification method and set of spray parameters could result in improving the coating bonding strength significantly. The electrical and thermal analyses of the coated samples also showed that the coated samples have a high capability in the generation of heat and acting as a heating element.

Keywords: Thermal spray coating; Plasma spraying; Glass fiber-reinforced polymer composite; Heating element; De-icing

Acknowledgments

It is a great pleasure for me to acknowledge Concordia University for supporting and providing me with the opportunity to pursue my post-graduate study at this amazing university.

First and foremost, I would like to express my special thanks to Prof. Christian Moreau, Prof. Mehdi Hojjati, and Prof. Ali Dolatabadi, my wonderful supervisors, for their assistance, ideas, feedback, and financial support during my MASc program. Without their help, this work would never have been possible.

Secondly, it is a pleasure to express my thanks to all my friends in thermal spray and composite groups, Concordia research staffs, especially, Dr. Daniel Rosca, Dr. Fadhel Ben Ettouil, Dr. Navid Sharifi, Omid Agababei, Gilles Huard, Nima Hamed Baradaran, and Mohammadhossein Ghayour. I deeply appreciate their helpfulness and willingness in providing useful information for this study.

Lastly, I wish to express my sincere gratitude to my family for their encouragement and moral support.

Table of Contents

List of Figures

List of Tables

Abbreviations

A	cross-sectional area
b	Width
CFRP	Carbon fiber-reinforced polymer
d	Thickness
FRP	Fiber-reinforced polymer
GFRP	Glass fiber-reinforced polymer
I	Electrical current
l	Length
PMC	Polymer matrix composite
ρ	Electrical resistivity
P	Electric power
R	Electrical resistance
R_s	Sheet resistance
t	Time
T	Temperature
V	Electrical voltage

Chapter 1: Introduction

1. Introduction

In the last decades, the application of polymer-based composite materials in different industries, especially the aerospace industry, has been increased significantly due to their specific characteristics such as high strength-to-weight ratio. However, composites development and further substitutions for some applications are limited due to their low thermal and electrical conductivity, poor abrasion resistance, and relatively low service temperatures [1-3]. Deposition of coating using thermal spray processes has always been an appropriate candidate for improving the mechanical, physical, and tribological properties of materials. However, there are some serious challenges associated with the coating of polymeric composite materials using thermal spray methods. These challenges include the vulnerability of composite materials to high temperatures and the impact of high-velocity particles, as well as their low surface free energy, which makes the deposition of coatings with high adhesion strength difficult. Limited research works have been done about coatings on composite materials and, in many cases, the coatings have shown low quality and uniformity. The purpose of this research work is to develop an electro-thermal de-icing element (heating element) for the composite structures that are exposed to cold and harsh weathers (e.g. aircraft and wind-turbines) by deposition of a metallic coating using thermal spray techniques. In the two following sections, different systems used for de-icing purposes, as well as methods and techniques that have been used up to now for the deposition of a coating onto composite materials will be discussed.

1.1. De-icing Systems

De-icing is a series of processes or equipment in which the ice or snow accumulated on a surface is removed. Several methods have been used for de-icing purposes in wind-turbines and aerospace industry. Some of these methods are commercially available, while a large number of them are immature and need more investigation to be implemented in the different industrial applications [4]. The most common de-icing techniques, especially in the aerospace industry, are as follow: 1) bleed air de-icing system, 2) electro-mechanical de-icing systems, 3) weeping wings, 4) pneumatic boot system, and 5) electro-thermal de-icing systems.

1.1.1. Bleed Air De-icing System

Bleed air system is the most common de-icing method in jet aircraft for keeping the aircraft surface temperature above the temperature required for ice formation and accumulation. In this system, hot air is ducted via the engine bleed valve from the compressor stage within the engine. The air then runs through a pre-cooler to reduce its temperature to 200 °C. This cooled air is then distributed using the bleed ducts to the different parts of the airplane like the wing anti-ice and deice systems. The hot air is then guided along the wing through telescopic pipes into a piccolo tube for distribution and warming up the slats. After that, the holes placed in the lower surface of the aircraft wing exhaust the used bleed air [5].

1.1.2. Pneumatic De-icing Boots System

Pneumatic de-icing boots system is another de-icing method used widely in the aerospace industry. These de-icing boots were invented by Goodrich in 1923. This system is also based on bleed air supply extracted from the airplane engines. The pneumatic boots are usually made of layers fabric-reinforced synthetic rubber, and a number of air chambers between the rubber layers. This system is usually placed on and attached to the leading edge, vertical stabilizer, and horizontal stabilizer surfaces to be de-iced. In this system, the ice accumulated on the boot surface is removed mechanically by alternately inflating and deflating the boot air chambers. In fact, the inflation and deflation of the chambers de-bonds the ice from the surfaces and breaks them into smaller particles, and after that the aerodynamic forces make the aircraft surfaces free of ice. Figure 1.1 shows a pneumatic de-icing boot before and after inflation. The pneumatic boots thickness is usually less than 1.9 mm. They also need low power for de-icing. It is also important that some ice layers be accumulated over the boot before turning on the de-icing boots system. In fact, the problem associated with many of pneumatic boot systems is the formation ice bridging. In ice bridging, an arch of ice is formed on top of the boot that is not removed easily by the air chamber inflation. However, this problem is solved in most of the modern de-icing boots by improving the inflation and deflation speed [6, 7].

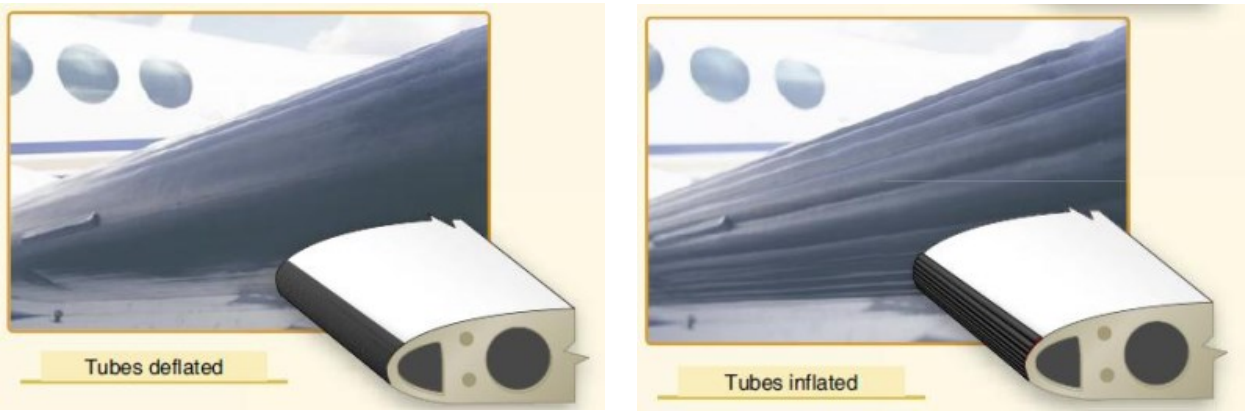

Figure 1.1: Pneumatic de-icing boot before and after inflation [7].

1.1.3. Weeping Wings De-icing System

Weeping wings system, also know as fluid ice protection system and Tecalemit-Kilfrost-Sheepbridge Stokes (TKS) system, is a fluid-based de-icing method. In this method the surface of the aircraft components that are prone to icing is coated with a fluid, known as freezing point depressant (FPD), to prevent from ice accumulation. Most of the de-icing fluids are composed of Ethylene-glycol. In this system, the super-cooled water droplets get mixed with the PFD liquid once they reach to the aircraft surface and form a mixture with a melting point lower than the ambient temperature [6].Laser-drilled titanium porous panels are used for distributing the FPD liquid to the aircraft leading edge [8]. The FPD liquid can also be distributed to the propellers and windshield using a slinger ring and spray bar, respectively [7]. Weeping wing systems can act as both de-icing and anti-icing. The fluid acts as an anti-icing system in the low and moderate icing conditions. However, it acts as de-icing in severe icing condition. In this situation, once the ice accumulates and creates bonding with the surface, a flow of the FPD liquid is pumped into the surface-ice interface for weakening the ice bonding. After that, the ice will be removed from top of the surface by aerodynamic forces [6].

1.1.4. Electro-mechanical Expulsion De-icing System

Electro-mechanical Expulsion De-icing System (EMEDS) is another technique used in an in-flight aircraft for de-icing purposes. In this system, a mechanical force is used for removing the ice over the aircraft surfaces [4, 9]. EMEDS was developed for the first time by Cox and Company, Inc. Based on their definition, in an EMEDS, “A millisecond-duration high current

electrical pulse delivered to the actuators in carefully controlled timed sequences generates opposing electro-magnetic fields that cause the actuators to change shape rapidly. This change of the actuator shape is transmitted to the erosion shield of the leading edge assembly causing it to flex and vibrate at very high frequencies. This rapid motion results in acceleration-based debonding of accumulated ice on the erosion shield", [10]. EMEDS are made of three units: 1) a De-icing Control Unit (DCU) which is used for timing and system control, 2) Leading Edge Assembly (LEA) which includes actuators mounted in a structure, and 3) Energy Storage Bank (ESB) which is used for delivering high current electrical pulses[10]. A schematic of this de-icing system is shown in Figure 1.2a.

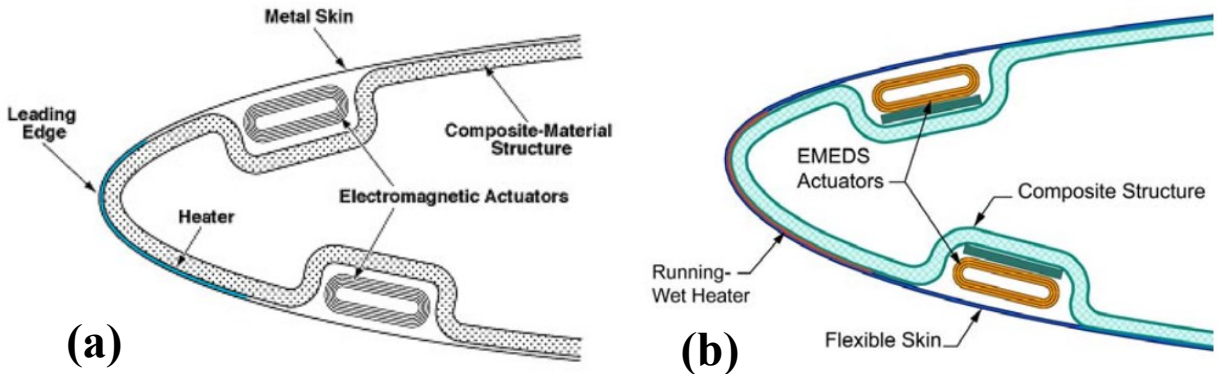

Figure 1.2: (a) Electro-mechanical Expulsion De-icing System (EMEDS), and (b) Thermo-Mechanical Expulsion De-icing System (TMEDS) [4, 9].

Hybrid Electro-mechanical Expulsion De-icing System, also known as Thermo-Mechanical Expulsion De-icing System (TMEDS), is a modified version of EMEDS, in which an EMEDS de-icer and electro-thermal anti-icer (electrical heating element) are combined with each other for improving the ice and snow removal efficiency. This de-icing system was also developed for the first time by Cox and Company, Inc. In this system, the electrical heater prevents from ice formation and accumulation, and the EMEDS removes the ice accumulated over the surface during or after the heating period. A schematic of TEMEDS is shown in Figure 1.2b.

1.1.5. Electro-thermal De-icing System

Electro-thermal de-icing systems use electrical resistance heaters in different forms like wire, film, or foil for heating and de-icing the components of an airplane or wind-turbine [6]. The electro-thermal heaters start heating the components as soon as an electrical current is applied to them. Figure 1.3 shows a kind of electro-thermal de-icing element used in aircraft. This de-icing-element is comprised of continuously heated spanwise and chordwise parting strips, as well as cyclically heated areas. The parting strips divide the total heated area into smaller sequentially heated parts. The partings strips also prevent ice-bridging from one shedding area to another area. This configuration and parting strips lessen the total instant power required for removing the accreted ice [6]. The electro-thermal systems can be used as both anti-icer and deicer. Indeed, they act as anti-icer when the heaters work continuously and prevent ice formation and accumulation, and they act as deicer when the heaters work intermittently to remove the ice accreted on the key surfaces of the aircraft or wind-turbine [11]. Usually, the application of electro-thermal systems as de-icing is preferred given that it just needs to melt a thin layer of the ice contact area to remove the accreted ice, and consequently the energy consumption in the de-icing is considerably lower [11]. It should also be noted that controlling the amount of heat generated using this de-icing method is very important. If the amount of generated heat is notenough, the ice layers may not shed as required, and in the case that the amount of generated heat is very high, too much melting will occur resulting in the formation of runback ice which is undesirable [6].

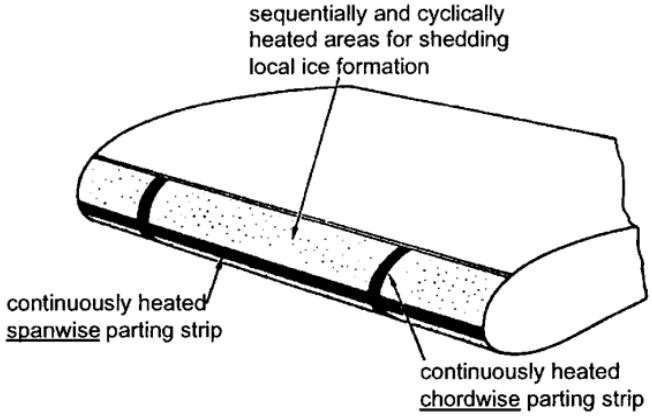

Figure 1.3: A typical electro-thermal de-icing system [6].

Composite materials comprise a high percentage of aircraft and wind turbines structures. As these composite structures are often exposed to harsh and cold weathers, designing a de-icing system for them has a high level of importance. An electro-thermal de-icing-element for composite structures can be fabricated by incorporation of a conductive metallic layer to them. Nickel and Chromium alloys (Nichrome) are among the most common alloys used for this purpose as they are conductive and have relatively high resistivity compared to pure metals. It is also worth noting that a thin adherent layer of chromium oxide forms on top of these alloys when they are heated up for the first time. This oxidized layer protects the underneath materials from more oxidation [12].

The purpose of this research work is the fabrication of an electro-thermal de-icing element by coating of the composite materials with a conductive material (i.e. NiCrAlY) using thermal spray techniques. In the next section, thermal spray processes will be discussed in detail.

1.2. Coating of Composite Materials and Thermal Spray Techniques

Thermal spray is a group of techniques and processes used for the deposition of a metallic or non-metallic coating onto a substrate. Based on the source of energy used for heating up and melting the coating materials (in the form of powder, wire, rod, ceramic, or molten materials) thermal spray processes can be divided into three categories in which heating and energy is provided by: (1) combustion, (2) dissipation of electrical energy, or (3) high-pressure gases (in the case of cold spray) [13].Once the coating materials are heated up, they are accelerated toward a substrate using process gases and form a bond with the surface. The subsequent particles will be making a bond with the already deposited particles and forming a lamellar structure [14].The most common and important processes for generating thermal spray coatings can be listed as follows: a) Air Plasma Spraying (APS), b) Vacuum Plasma spraying (VPS), c) High-Velocity Oxy-Fuel Spraying (HVOF), c) High-Velocity Air Fuel (HVAF), d) Arc Spraying (AS), e) Flame Spraying (FS), f) Detonation-Gun Spraying (D-GUN), and g) Cold-Gas Spraying Method (CGSM) [15]. In a thermal spray process, different factors may affect the coating properties, including the coating materials, the form of coating materials, and the substrate properties. Besides these factors, the thermal spray gas temperature (flame temperature) and the particles impact velocity have a critical role in determining the coating properties [13]. Figure 1.4 depicts

flame temperature, and particle velocity ranges for different types of thermal spray processes [16].

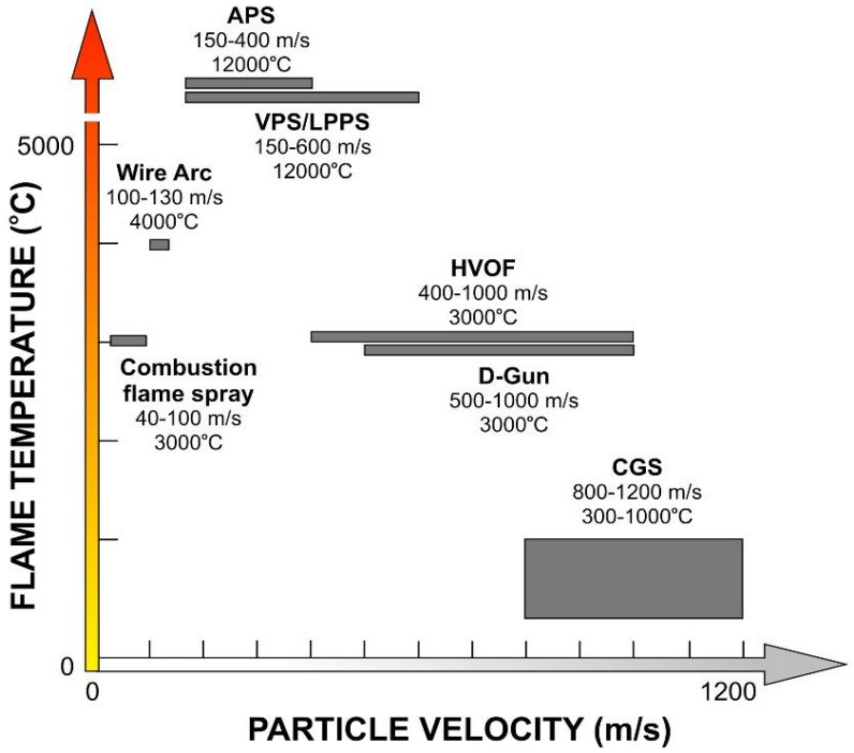

Figure 1.4**:** Particle impact velocity and gas temperature in different thermal spray processes [16].

Thermal spray processes are widely used for enhancing thermal, physical, mechanical, and tribological properties of metallic substrates. However, the coating of composite materials using thermal spray methods is associated with some serious challenges. As mentioned earlier, in polymer-matrix composites (PMCs), service temperature is relatively low, usually less than 300 °C while in most of the thermal spray processes, temperature ranges are very high (see Figure 1.4). In addition, composite materials are brittle, and the impact of high-velocity particles would break the composite fibers and result in degradation and appearance of many cracks in the composite surface. However, in a thermal spray process, especially cold spraying, the particle velocity range is usually very high. Furthermore, given that polymeric materials are chemically inert[17] in comparison to the metallic materials, deposition of a metallic coating with high

uniformity and adhesion would be very difficult [14]. In the following subsections, the different surface preparation methods used for preparing the substrates before the coating deposition process, as well as the thermal spray techniques have been used up to now by researchers for coating of fiber-reinforced polymers (FRPs) will be discussed. It is also worth noting that unlike the coating of metallic substrates, limited research works have been conducted about the coating of composite materials.

1.2.1. Substrate Preparation

Preparing the substrates prior to the coating deposition process is a very important and vital step for improving the bonding and adhesion strength of thermally-sprayed coatings. Generally, substrate preparation is made of three steps [13].

The first step is cleaning the substrates from contamination. In this step, different methods like vapor degreasing and solvent rinsing are used for making the substrates surfaces free of contamination (e.g. oil, grease, and organic compounds) [13].

The purpose of the second step is making the surface rough and increase its surface energy for improving the adhesion during coating deposition. Grit blasting is one the most common and effective surface preparation methods used for roughening the surface of metallic substrates in which the substrate surface is bombarded with high-velocity abrasive particles like SiC or alumina grits. More details about this method are presented in the next chapter. However, this method is not very useful for roughening the composite substrates as the impact of high-velocity grit blasting particles damages the fibers and removes a lot of composite layers easily. So, for composites, or generally polymeric substrates, this method might not be applied without a surface modification prior to the grit blasting. For example, Liu et al. [18] and Guanhong et al. [19] used grit blasting for preparing the carbon fiber-reinforced polymer composite substrate (CFRP) prior to the spraying of Al and Zn by using plasma spraying technique. As shown in Figure 1.5, the CFRP fibers have been damaged and broken due to grit blasting, and even some of them have penetrated to the coating structure. It should also be noted that by increasing the grit blasting carrier gas pressure, more damage will be induced to the composite substrate.

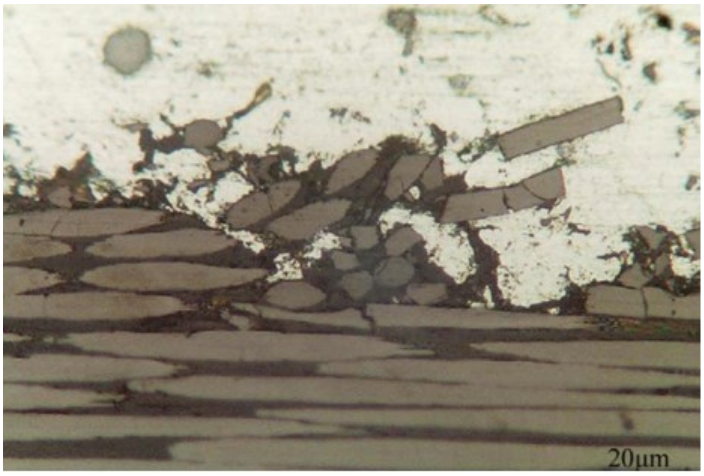

Figure 1.5: A grit-blasted CFRP substrate after coating with Al [18].

Using abrasive papers is another method used for preparing and roughening the composite substrates. Abrasive papers increase the surface roughness by removing the composite resin. The disadvantage of this method, especially when it is applied manually to the substrate surface, is that the surface roughness is not uniform. In addition, similar to grit blasting, using this method may damage and break the composite fibers, and induce adverse effects on the mechanical properties of the composite substrate. To determine the effects of using abrasive paper on the mechanical properties of the coated composite substrate, Liu et al. [2, 18] compared the shear bond strength of the coatings prepared using grit blasting with the coatings prepared using abrasive papers. In that experiment, all the coatings were deposited using a cored wire composed of steel skin and Ni–Cr–B–Si as filler material and by plasma spraying technique. The grit blasting was done using two types of powder, 28 and 46 mesh corundum, and with the grit blasting carrier gas pressures of 0.2, 0.4, 0.6, and 0.8 MPa. In the case of preparing by abrasive papers, 60, 80, 100, 180, 360, 600, and 1000 mesh abrasive papers were used for grinding the composite substrates before the coating process. After analyzing the coated samples, they found that the sample grit-blasted using 28 mesh corundum and with the carrier gas pressure of 0.2 MPa has the highest shear bond strength (about 9.4 MPa) among all the coated samples. However, in the case of samples prepared using abrasive papers, the maximum bonding strength was achieved using the 100 mesh abrasive paper, in which the maximum bonding strength value

was about 4.8 MPa (about half of the bonding strength of the sample grit-blasted with the gas pressure of 0.2 MPa). These results show that the surface roughness in the grit-blasted samples is higher, which makes it easier for the molten particles to lock into the composite surface and fully adhere during the coating deposition. So, not only does using abrasive papers damage the composites and fibers but also it results in relatively weak mechanical properties. They also observed that by increasing the grit blasting carrier gas pressure, the bonding strength decreases due to inducing more damages to the substrates during grit blasting.

Chemical treatment is another method that has been used for preparing the CFRP substrates prior to the coating deposition process. In this method, the substrates surface energy is increased by placing them in the exposure of chemical materials and solutions. Ganesan et al. [20] did an investigation for determining the effects of surface preparation methods on the air-plasma-sprayed Cu coatings adhesion strength and quality. In that study, the CFRP substrates were treated mechanically, thermally, and chemically. In thermal treatment, substrates were exposed to the plasma plume before starting the coating process. In the case of chemical treatments, the surface of the substrate was first treated using an aqueous solution containing 25 vol.% 2-(2-butoxyethoxy)ethanol for 10 minutes, and then they were treated by $KMnO_4$ for about 10 minutes. After that, the samples were exposed to a 1 M solution of trichlorotriazine in toluene at 60 °C for about 24 hours. Finally, in the case of mechanical treatment, samples were grit-blasted using steel grits with a size of 0.71 mm. Once the substrates were coated and analyzed, it was found that using those chemical treatments result in better coating adhesion strength and quality compared to the two other preparation methods (see Figure 1.6). It is also was reported that the higher coating adhesion is due to the notably higher surface energy in the substrate treated chemically in comparison to those treated thermally and mechanically.

Other methods, like the incorporation of granular particles on top of the polymeric substrates, have been used for roughening and activating the composite substrates [21-29]. Some of these methods are discussed in the next subsections.

Finally, after roughening and activating the surface of the substrates, they should be cleaned using compressed air or ultrasonic baths for keepings substrates surface free of any grit and contamination after grit blasting. The presence of grit may create a defect at the interface of the coated sample [13].

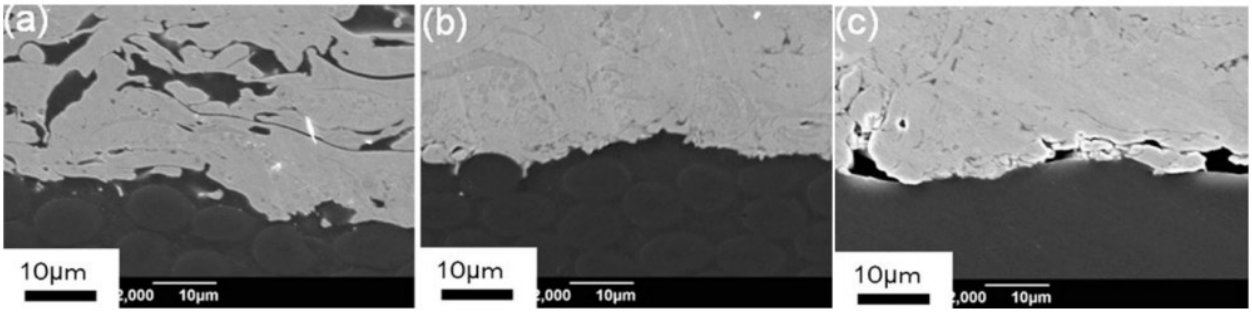

Figure 1.6: The cross-section of Cu-coated CFRPs treated (a) mechanically, (b) chemically, and (c) thermally [20].

1.2.2. Flame Spraying

Flame spraying is the first thermal spray technique, in which a hot flame for melting the coating materials is generated using the chemical energy of combustion of the fuel gas in oxygen [15].Figure 1.7 depicts the schematic of a flame spray torch. In flame spraying, the working gases (oxygen and fuel) enter the torch axially. The coating materials (in the form of powder, wire, or rod) are introduced axially or perpendicularly to the combustion flame by using a carrier gas. Once the coating materials melted, the mixed gases accelerate the molten particles toward the substrate [15, 30].

The most important advantages of using flame spraying, especially for the coating of polymeric materials which are vulnerable to the impact of high velocity and temperature particles, are its relatively moderate flame enthalpt and low particle velocity in comparison to the other thermal spray processes [15]. However, the coatings deposited using this method have usually high porosity (in the range of 16-19%), which results in degradation of the coating mechanical properties [15]. Some research works about the coating of composite materials using the flame spray process have been done up to now. For instance, Loperal et al. [28, 29] investigated the coating of glass fiber-reinforced polymer composites (GFRPs) by using flame spraying method to fabricate a heating element for de-icing applications in aircraft and wind turbines. They first fabricated a GFRP plate by stacking of 20 unidirectional GFRP prepregs. Once the composite plate was prepared, it was cut into smaller samples. After that, a layer of high strength epoxy adhesive and #220 grit garnet sand (with the chemical formula of

$Fe_3Al_2(SiO_4)_3$) mixture was applied on top of the composite substrates manually for increasing the surface roughness, and consequently improving the coating adhesion. Following this, a layer of NiCrAlY coating, as heating element, was deposited onto the composite substrates using flame spraying. The cross-section of NiCrAlY-coated sample is shown in Figure 1.8. The substrate and fibers are undamaged and in good condition. However, the sand-epoxy and coating layers are not uniform, and the absence of coating can be seen in some parts. In addition, as this coating is used as heating element, the non-uniformity of the coating may contribute to non-uniform temperature distribution along the coating surface and formation of hot and cold zones at the same time in the different parts of the coating. In another similar study, Gonzalez et al. [22] sprayed an Al-12Si coating layer onto a GFRP substrate by utilizing flame spraying. In that work, in order to roughen the substrate surface and prepare it for the coating deposition, a layer of #80 garnet sand was incorporated on top of the resin-wet fibers during the manufacturing of the composite tubes (before vacuum-bagging and the curing process). The result of their coated sample cross-section indicates that similar to the previous study, the coating is not uniform. Other studies [21, 22, 24, 27-29, 31] also show that the coated-composite samples that were prepared by addition of garnet sand and coated using the flame spraying method do not have a uniform coating structure. So, it might be concluded that usually using flame spraying method for the deposition of a metallic coating onto a composite sample treated by addition of granular particles (especially garnet sand) does not result in the formation of a coating with high uniformity, quality, and deposition efficiency.

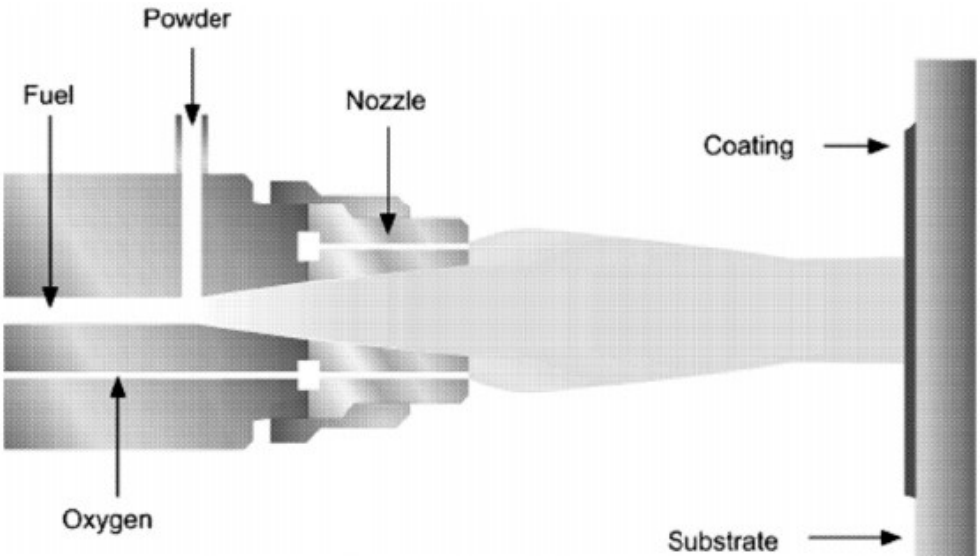

Figure 1.7: Principle of flame spraying using powders [30].

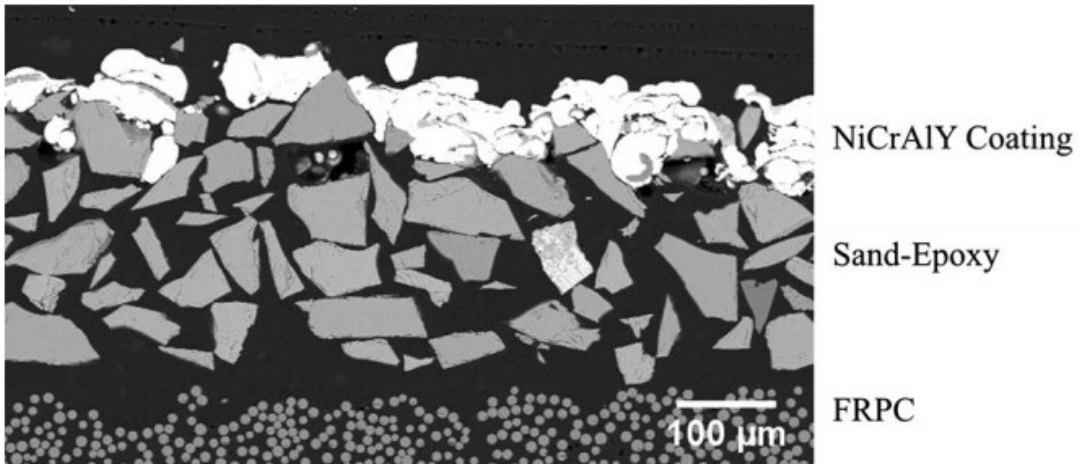

Figure 1.8: Cross-section of a NiCrAlY coating deposited onto a GFRP sample using flame spraying [28].

1.2.3. Arc Spraying

Arc spraying is another thermal spray method in which two metallic wires are used as the coating material. In this process, as shown in Figure 1.9, the metallic wires are electrically charged and fed into the arc wire spray torch. An electrical arc is formed between the tip of the metallic wires. The electrical arc heats up and melts the wires. After that, the compressed air (atomizing gas) atomizes and accelerates the molten droplets toward the substrate [15, 30].

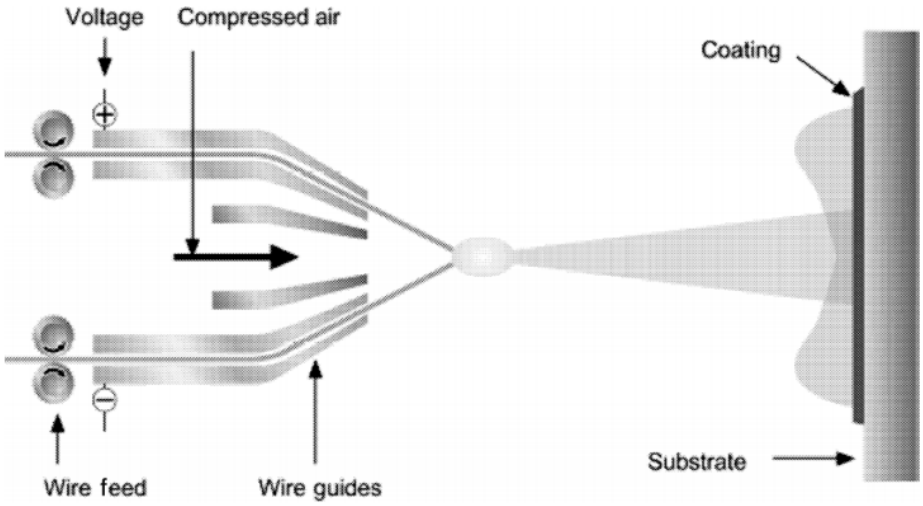

Figure 1.9: Schematic of an Arc spray torch [30].

Very limited research studies have been conducted up to now about the metallization and coating of polymer-based materials using arc spraying technique. This might be attributed to the fact that in this process, for the formation of liquid metal droplets and spraying them onto the composite substrate, the temperature of the tip of the metallic wires should go over the melting point of the wires, and in fact the droplets are overheated. So, although the range of gas temperature in other thermal spray processes like plasma spraying might be higher (see Figure 1.4), the temperature of the molten droplets and the amount of heat that these droplets transfer to the substrates are usually higher in the arc spray process compared to the other thermal spray processes. Generally, the thermal spray processes in which the coating materials are in the form of wires or rods result in higher surface temperatures and more mechanical degradation (in the case of using polymeric substrates) during spraying in comparison to the processes that are fed by powder as coating material [2, 18]. Liu et al. [18] carried out a study for comparing the mechanical properties of the coatings sprayed using arc spraying with those sprayed by air plasma spraying. In this study, carbon fiber-reinforced polyimide composites were used as substrate. In the first step, the substrates were cleaned by acetone and grit-blasted using corundum powder. After that, the arc spray process was used to spray Zn and Al wires, and the plasma spray process was used for spraying Zn and Al powder onto the CFRP substrates. The shear adhesion strength test results showed that the adhesion strength of plasma-sprayed Al, plasma-sprayed Zn, arc-sprayed Al, and arc-sprayed Zn coatings are 12, 11, 7.5, and 10.5 MPa, respectively. It can be seen that the plasma-sprayed Al coating has the highest adhesion strength, while the arc-sprayed Al coating has the lowest adhesion. These results might be explained by the fact that during arc spraying, due to impact of overheated molten droplets, the substrate surface temperature was increased significantly (over the service temperature of the composite) for a long time, and this caused more damages to the coating-composite interface and more degradation in its mechanical properties like adhesion strength. Interestingly, unlike Al coating, the adhesion strength values of arc-sprayed Zn coating and plasma-sprayed Zn coating are very close to each other. It is due to the fact that Zn has a low melting point (419.5 °C), and even when it is sprayed in the form of wire by arc spraying, it does not increase the composite temperature over its service temperature, and consequently does not induce significant damage to the substrate surface. However, in the case of Al, the melting point (660.3 °C) was about 50% higher than that of the Zn.

1.2.4. Cold Spraying

Cold spraying is a kinetic-based process in which supersonic jets of compressed gases are used for accelerating the powder particles to high speeds (i.e. between 300 and 1500 m/s) toward the substrate. The unmolten particles with in-flight velocities of over 500 m/s deform plastically and consolidate on impact with the substrate to form a coating layer [13, 32]. The acceleration of the coating materials to supersonic velocities and therefore high kinetic energies are achieved using convergent-divergent nozzles known as de Laval nozzle [33]. The coating adhesion in cold spray process is provided by the plastically deformation and interlocking of the deformed particles once they impact the substrate [31]. Figure 1.10 illustrates the schematic of a cold spray system. In this process, N_2, He, or their mixtures is usually compressed up to 3.5 MPa and heated up to 600-800 °C by using a heating coil. Once the working gas was introduced to the de Laval nozzle, it expands to supersonic velocities [15]. At the same time, the powder is injected into the nozzle throat, and particles are heated up to temperatures below the melting point and accelerated to high velocities [15]. In the cold spray process, particles adhere onto the substrate and form a coating layer only if their impact velocity be higher than a critical value, which is called critical velocity. The value of critical velocity depends on the material of the powder and substrate and is typically in the range of 500-900 m/s. The powders used in this process as coating materials are usually very fine (the mean diameter size of the particles is in the range of 1-50 μm) [13].

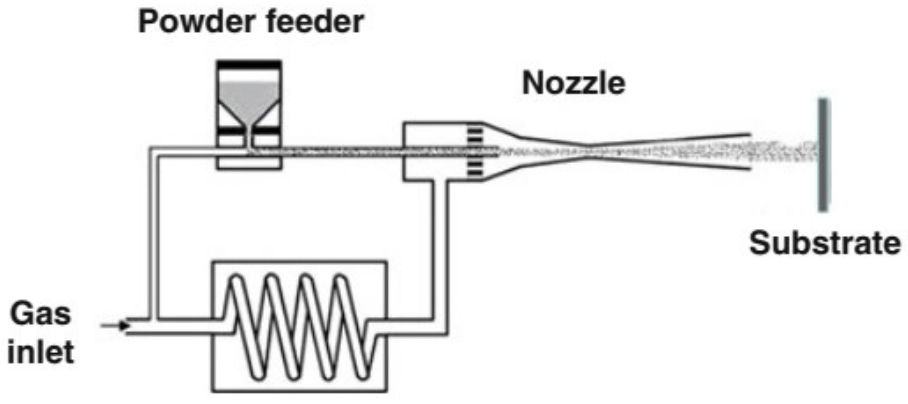

Figure 1.10: Schematic of a typical cold spray system [33].

The gas temperature in cold spray usually does not exceed from 1000 K. This could be considered as an important advantage for the deposition of coatings with low oxidation level, and metallization of those kinds of PMC substrates which are sensitive to high temperatures. However, as the coating adhesion in this process is based on the kinetic energy of the particles, the range of particle impact velocities is very high, which may induce significant damage to the composite substrate. The damage is more severe and critical when the composite matrix is made of thermoset materials as thermosets are brittle and impact of high-velocity particles not only break the fibers but also results in the formation of cracks and micro-cracks in the interface of composite substrate and coating. Cold spray technique has been used more for coating of thermoplastic-based composites [25, 34-38]. However, in many of these cases also a significant amount of substrate erosion and degradation have been reported [34]. Cold spray processes can be classified into two main types: low-pressure cold spray (LPCS) and high-pressure cold spray (HPCS). In the LPCS process, the gas pressure is typically less than 1 MPa, and the particle impact velocity is in the range of 300-600 m/s [13, 31, 39, 40]. In the HPCS process, the gas pressure is in the range of 1-5 MPa, and the particle impact velocity is relatively very high and in the range of 800-1400 m/s [13, 31, 39, 41]. The deposition efficiency in the LPCS process is usually low as the kinetic energy of the particles is not enough for the formation of a uniform coating, especially when the substrate is made of polymeric materials. On the other hand, in the HPCS process, the particles have high momentum and kinetic energy. In this case, the particles can damage the composite substrate and even sometimes penetrate into the composite structure. Lupoi et al. [40] did a study about the possibility of deposition of copper, aluminum, and tin coatings onto polymeric substrates, including PC/ABS, polypropylene, polystyrene, polyamide-6, and GFRP, using cold spray technique. It was found that in all cases, the impact of copper particles resulted in contact stresses, and consequently, degradation and erosion of the polymeric substrates. In addition, it was found that using aluminum powder as the coating material, due to its low specific weigh, does not lead to a notable amount of surface erosion. However, as the velocity of the aluminum particles was lower than its critical velocity, no coating was formed and deposited onto the substrates. Finally, a thin layer of Tin coating (45-100 μm) was deposited successfully just on top of the thermoplastic substrates. However, it should also be noted that tin is among the metallic materials that have the lowest melting points, and even in a process like

cold spraying, its particles may melt during spraying, and this ease the formation and deposition of the tin coating onto all type of substrates even polymers and composites.

HPCS process also has been used for embedment of metallic particles (discontinuous coating) into the thermoplastic materials [31, 37, 42] . For example, Vucko el al. [42]embedded copper particles into high-density polyethylene (HDPE) and nylon using cold spray process for determining its application as an antifouling system. It was found that unlike Cu-embedded nylon, Cu-embedded HDPE has a very decent performance. They also found that antifouling success is related the cold spray process parameters (which have a direct influence on the particle embedment depth), and the type of the thermoplastic (which affects the interaction between the substrate and copper particles).

1.2.5. HVOF Spraying

High-velocity oxygen-fuel (HVOF) is a kind of thermal spray processes with the capability of fabrication of coatings with advanced and unique properties [30].Figure 1.11 shows the schematic of an HVOF torch. In this process, the combustion is initiated inside the chamber by generation of an ignition. The exhaust gas, formed by the nozzle, passes through a converging diverging nozzle and exits into the atmosphere. The powder also is introduced axially or radially into the gas jet [15].

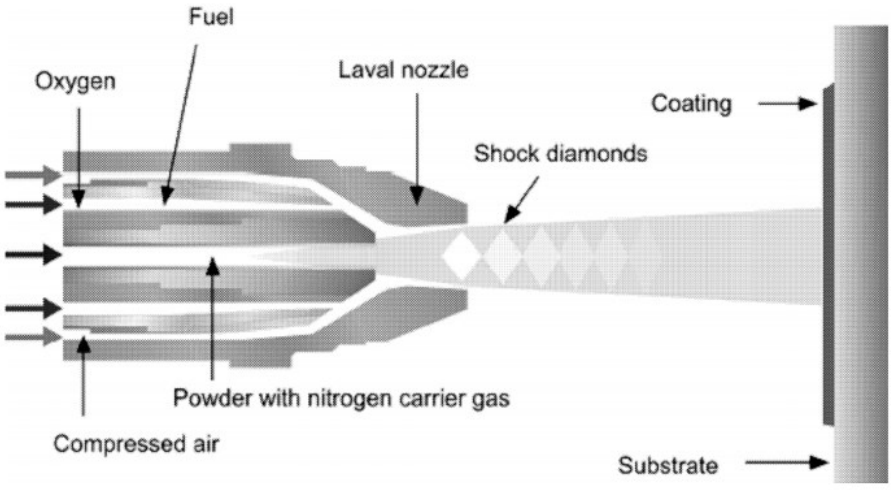

Figure 1.11: The schematic of and HVOF torch [30].

HVOF process is widely used for coating metallic substrates. The gas temperature and particle impact velocity in this process are in the range of 800-2300 K and 400-1100 m/s, respectively [15]. Due to the high velocity of particles and significant damage and delamination induced to the PMC substrates during the coating deposition process, only one research work has been published about the coating of composite and polymeric materials using HVOF technique up to now. In 2005, Ivosevic et al. [43, 44], investigated the feasibility of spraying functionally graded coatings (comprising a layer of pure polyimide, a layer of WC-Co + polyimide, and a layer of WC-Co as the last and top-coat) onto the CFRP substrates using a combination of HVOF and flame spray processes for improving the erosion and oxidation resistance of polymer-based composites. The first two coating layers were deposited using the HVOF process, and the last coating layer, pure WC-Co, was deposited using flame spraying. After analyzing the samples, it was found that the amount of substrate and coating crack, as well as fiber breakage in the interface of coating and substrate (even in the cases in which the composite substrates were not grit-blasted), are high and significant. In fact, in all cases, considerable damage was induced to the polymeric substrate. Globally, HVOF is considered as an inappropriate method for the coating of polymeric materials as both the gas temperature and particle impact velocities are relatively high in this process.

1.2.6. Plasma Spraying

Plasma spraying is one of the most common thermal spray processes used widely in the different industries for the fabrication of coatings with different applications. As shown in Figure 1.12, a plasma torch comprises an anode, made of copper, as well as a cathode made of tugsten. An electrical arc is formed inside the torch between anode and cathode. The electrical arc ionizes and heats up the plasma gas injected at the base of the cathode, and then a high temperature and velocity plasma jet exits the torch. At the same time, the powder injected into the plasma jet, melt and reach to the substrate surface at a high velocity [30]. As plasma spraying was used in this research work for the deposition of coating onto GFRP composite substrate, more details about this method are discussed in this subsection.

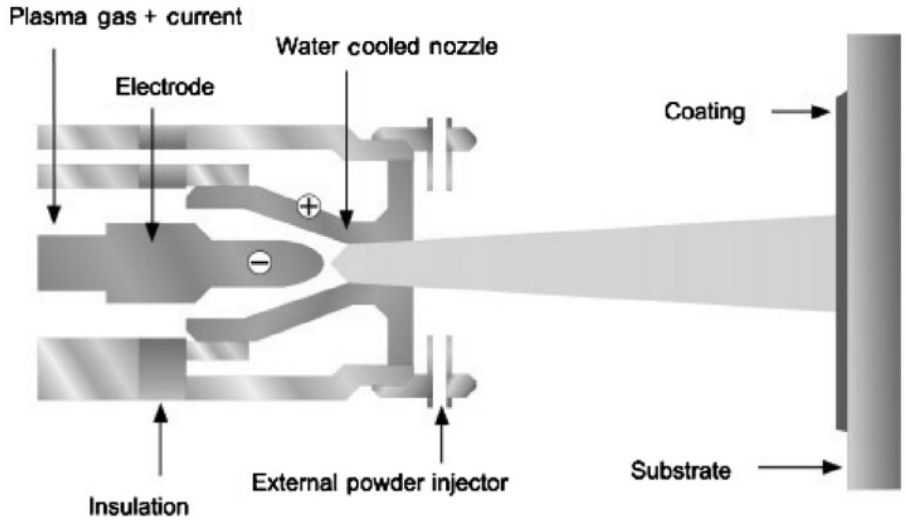

Figure 1.12: The schematic of a plasma spray torch [30].

Plasma spraying can be classified into three categories, which are: a) Atmospheric plasma spraying (APS), where the plasma jet is exiting into the air, b) Controlled atmosphere plasma spraying (CPS), where the plasma jet exits the torch into a controlled atmosphere chamber, and c) Low-pressure plasma spraying or vacuum plasma spraying (LPPS or VPS), where the jet is exiting into a low-pressure chamber (i.e. 10-30 kPa) [13]. Optimization of plasma spray process parameters is very important for achieving a coating with high deposition efficiency, and good quality and consistency [30]. Table 1.1 presents the most important parameters in a plasma spray process.

The particle impact velocity in a plasma spray process is usually in the range of 160-200 m/s. The plasma gas temperature is usually less than 12000 K [15]. By referring to Figure 1.4, it can be seen that in plasma spray processes, the flame temperature is higher than that of the HVOF and cold spray processes. However, the particle velocity in plasma spraying, especially in APS, is considerably lower compared to that of the HVOF and cold spray processes. So, for doing the coating deposition onto polymeric substrates using plasma spray method, it is very important to manage and cool-down the substrate temperature during spraying by utilizing an appropriate cooling system during spraying (e.g. using water-cooled sample holder, air amplifiers, and air blowers).

Table 1.1: Plasma spray process parameters [13].

	Torch	**Plasma jet**	**Particles**	**Substrate**
Input parameters	Plasma gas composition Current Nozzle design Cooling water flow		Morphology Feed rate Size distribution Carrier gas flow rate	 Substrate material Substrate treatment
Operating characteristics	 Voltage Voltage efficiency	Geometry Stability Temperature distribution Velocity distribution	 Particle trajectory T_p and V_p distributions	 Deposition efficiency Porosity Coating properties
	Torch set up	Pressure Atmosphere Humidity		

Among the different types of plasma spraying, only atmospheric plasma spraying has been used up to now for coating polymeric materials. It is also worth noting that in most cases, low melting-point metallic powders (e.g. Zn and Al) were used as the coating materials for spraying the PMC materials [1-3, 19, 45]. For instance, Guanhong et al. [19] utilized APS technique for the deposition of Al as bond-coat and Al_2O_3 as top-coat onto PMC substrates for enhancing their mechanical properties. The metallic coatings were sprayed onto several composite substrates using different spray parameters (different currents and spray distances). After examination of coated samples, it was found that the spray parameters play a very significant role in determining the microstructure, phase composition, and mechanical properties of the coated samples. The maximum shear adhesion strength achieved for the Al bond-coat was about 5.21 MPa. In another study, Liu et al. used plasma spraying for the deposition of Zn, Al, Cu, and Ni_3Al coatings onto CFRP substrates. After the coating process, the microstructure and shear adhesion strength of the coated samples were analyzed. The results demonstrated that deposition of Ni3Al and Cu leads to delaminations at the interface of substrate and coating due to the relatively high melting point of coating materials and low surface energy of the CFRP substrate. However, Al and Zn were deposited successfully. In addition, by comparing the plasma-sprayed Al and Zn with arch-sprayed Al and Zn, it was found that using plasma spraying results in fabrication of a coating with superior mechanical properties (more details about this comparison are discussed in section 2.3). In another interesting study, Affi et al. [46] used a combination of plasma spraying and cold spraying to deposit an aluminum coating layer onto CFRP substrates for the lightning protection application in aircraft. In that study, a thin layer of aluminum coating (about 15 μm) first was deposited onto the composite surface by using plasma spraying and, after that, cold spraying was used for the deposition of the second aluminum layer as top-coat. The plasma spray process was not used alone for the deposition of the whole coating due to the fact that the gas temperature in this process is high and it would increase the oxidation of sprayed particles, and consequently the electrical resistivity of the coating which is not desirable in the fabrication of a lightning protector coating. In addition, when the cold spray method was used alone for the coating of CFRPs, the coatings started peeling off once their thickness reached about 30 μm due to damages induced to the CFRPS surface by the impact of high-velocity particles. That was why a combination of plasma spraying and cold spraying was used for the fabrication of lightning protector coating.

1.3. Objectives

The main objective of this study is to develop a process for uniform deposition of a high-quality nickel-chrome-aluminum-yttrium (NiCrAlY) coating onto a polymeric glass fiber reinforced composite (GFRP) by using plasma spray technique for the de-icing and anti-icing applications in aircraft and wind turbines.

Other objectives of this study are also listed as follow:

- Discussing the challenges associated with the coating of polymeric materials and the factors that make the coating of PMCs different from metallic materials

- Using different preparation and surface modification methods for preparing the glass fiber-reinforced polymer (GFRP) substrates prior to the coating deposition process.

- Deposition of a NiCrAlY coating layer onto GFRP substrates, and analyzing the effects of spray parameters on the microstructure and quality of the coatings.

- Determining the effects of the NiCrAlY powder size distribution on the coating microstructure and propertiens.

- Finding a set of appropriate spray parameters (close to optimized parameters) for the deposition of the NiCrAlY coatings with high quality and uniformity.

- Determining and comparing the electrical properties of the coated samples.

- Analyzing the capability of the coated sample in generating power and heat once they are connected to a power source.

- Comparing the temperature profile of the coated samples when a specific amount of current is applied to them.

Chapter 2: Experimental Method

2. Experimental Method

This research project is made of seven steps including: 1) fabrication of glass fiber-reinforced polymer composites (GFRP) and cutting them into smaller samples, 2) substrate preparation 3) deposition of coating by using plasma spraying, 4) analysis of the microstructure of the coatings, 5) electrical characterization of the coated samples, and 6) analysis the performance of the coated composite samples as a heating element, and 7) determining the coatings adhesion strength. These steps are discussed in detail in the following sections.

2.1. Substrate Fabrication

In this step, three 1-by-1 foot plates were fabricated by using glass fiber-reinforced polymer prepreg plies (GFRP) and stainless steel mesh cloths. Prepregs are fibers impregnated with partially cured resin (e.g. epoxy) in the form of flexible sheets [47]. In the first step, the glass fiber-reinforced polymer prepregs (Cytec E773FR, 5 Garret Mountain Plaza, Woodland Park, NJ 07424 USA) were taken out of the freezer and left at the room conditions for about three hours. This allows the temperature of prepreg to rise to room temperature, and the viscosity is reduced so that the prepregs can be cut into smaller sheets easier. After that, the prepregs were cut into 12-by-12-inches square sheets (laminas). For making a 4 mm composite plate, 16 unidirectional GFRP plies (i.e. $[0_{16}]$ composite) were utilized. A tool was prepared for providing the shape and surface finish. Before transferring the laminas to the tool for making the composite plates, the tool was cleaned by acetone and a layer of release agent was applied on top of it for facilitating the removal of laminas and plates. Then, the 16 GFRP plies were aligned and stacked carefully for making each plate. Woven wire #200 and #400 stainless steel mesh cloths (type 316) were incorporated as an additional and top layer to the first and second plates, respectively. The properties of these steel mesh cloth are shown in Table 2.1, and their microscopic images are shown in Figure 2.1. The reasons and purposes of incorporation of these cloths to the composite plates will be discussed in detail in the next chapter.

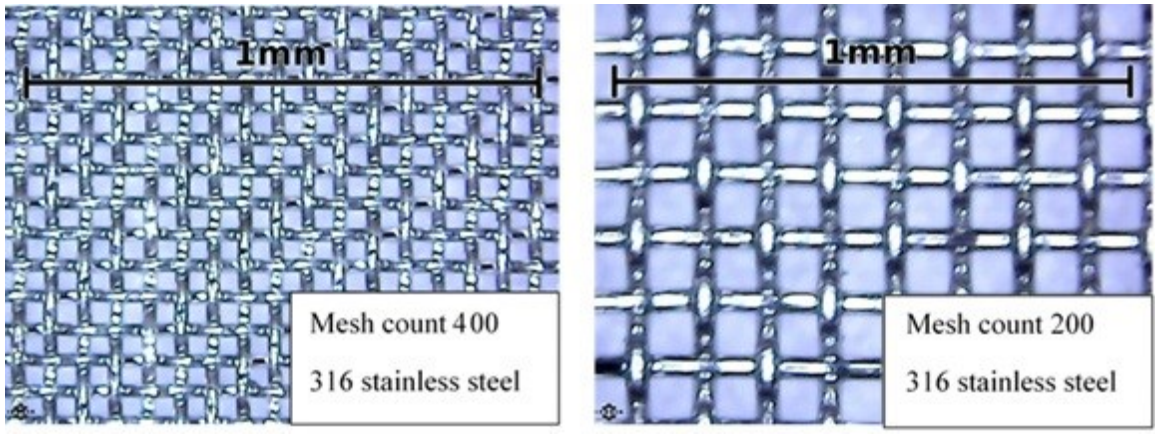

Figure 2.1: Microscopic images of 200 and 400 stainless steel mesh cloth [48].

Table 2.1: 200 and 400 stainless steel mesh cloths properties [48].

Mesh count	Nominal aperture	Wire diameter	Open area (%)	Weight kg/m^2
200	75 µm	60 µm	34	0.28
400	38 µm	30 µm	31	0.16

In the next step, for making composite plates with high strength to weight ratio, the tool and GFRP plates were vacuum-bagged. Vacuum bagging is a technique used to create mechanical pressure on a composite part during its cure cycle, and it is done by sealing of the composite plates from the air with vacuum bagging materials [49]. In fact, the purpose of vacuum bagging is to create pressure on the samples in order to accomplish two important objectives: first, to help the elimination of the air trapped between the prepreg layers as it can result in delamination, and second, to eliminate the excess resin from the parts. Vacuum bagging also improves samples physical properties as it helps to create a part with higher fiber to resin ratio in comparison to parts made with typical hand lay-up. Generally, the target fiber to resin ratio for most composite parts is about 1, and this is nearly impossible to achieve with typical hand lay-up.

The vacuum bag used in this experiment was made of four primary items, including vacuum bagging film, peel ply or release film, breather and bleeder cloth, and a vacuum pump. The vacuum bagging film was the outermost layer of the bagging set up used for creating the airtight seal and was stretched over the part and other vacuum bagging material. In this setup, sealant also was used for creating the airtight seal to close the bagging film to the tool (mold) and

enabling the vacuum to work. The peel ply was the other part of the vacuum bag used to ease the pulling away the part from the other bagging materials once the cure is complete. It was placed on the surface of the laminate. Breather and bleeder cloths were another part of the bagging set up that were put exactly beneath the vacuum bagging film. These cloths, in fact, serve two key purposes. Firstly, as a breather, these cloths facilitate airflow as channeled throughout the laminate. Indeed, once the vacuum connector sits directly on top of the breather, it pulls air as well as any gases released during the cycle from the part and through the cloth. Secondly, as a bleeder, these cloths absorb excess resin pulled from the part by the vacuum. Finally, for vacuuming the bag materials, the vacuum bagging film was connected to a vacuum pump using a hose and a vacuum connector. A schematic and summary of the function of different components of a vacuum bag are illustrated in Figure 2.2.

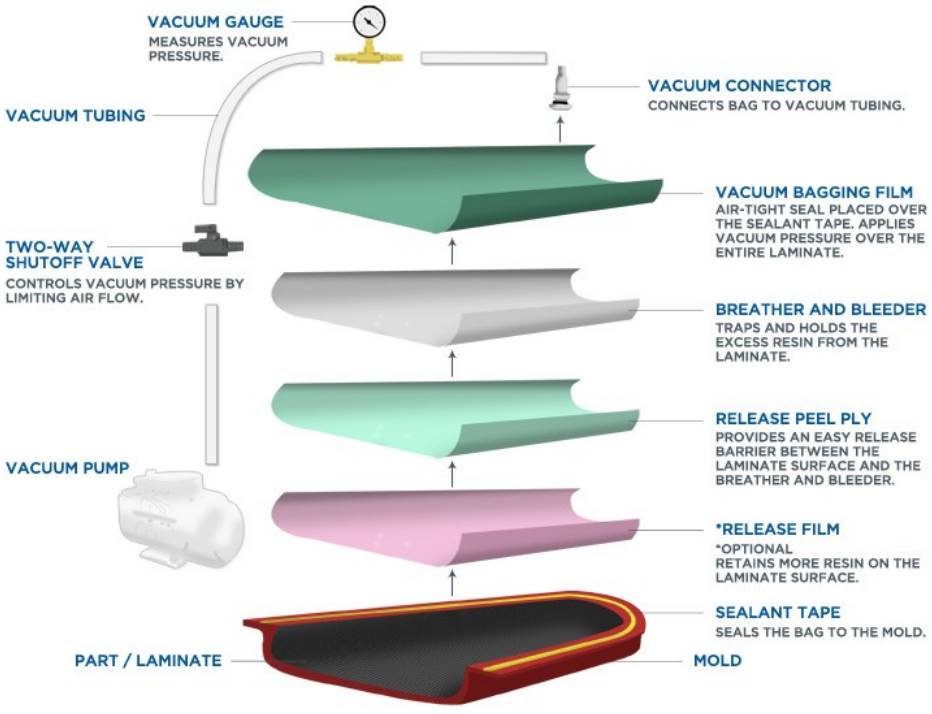

Figure 2.2: Schematic of a typical vacuum bagging lay up [49].

After vacuum bagging the tool and prepregs, the setup was transferred to an autoclave for the curing process. An autoclave is a pressure vessel used for applying relatively high pressure and temperatures needed for the fabrication of some parts and materials such as composite substrates. Figure 2.3 shows the heating cycle (curing cycle) used for the curing of the composite plate [50]. As it is shown in this figure, the heating cycle was made of three steps. First, the autoclave temperature increased from 24 to 127 °C (75 to 260 °F) with a slope of 2.7 °C/min (5 °F /min) in 37 minutes. The temperature then was constant in the range of 121-132 °C (250-270 °F) for about 100 minutes. Finally, the autoclave was cooled down with a slope of -2.7 °C/min (-5ºF/min) for about 30 minutes. Once the curing cycle was completed, the vacuum bag set was taken out of the autoclave, and the vacuum bag film was removed from top of the composite plates.

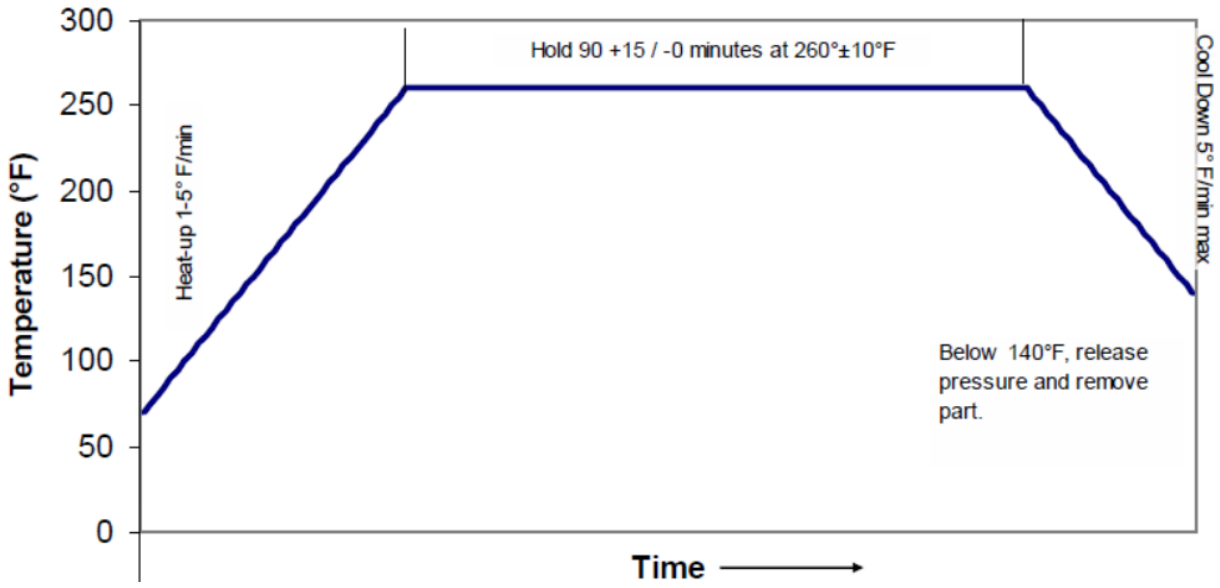

Figure 2.3: Recommended heating cycle for curing CYCOM E773FR prepregs [50].

After fabrication of composite plates, they were cut into smaller samples using a diamond saw. Figure 2.4 shows the fabricated composite plates.

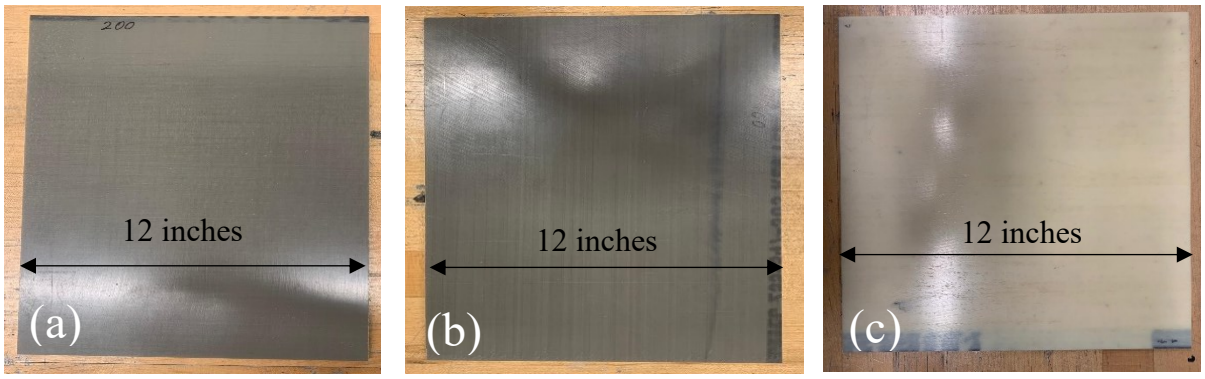

Figure 2.4: (a) 200 mesh plate, (b) 400 mesh plate, and (c) typical composite plate.

2.2. Substrate Preparation

Proper preparation of the substrates prior to the coating process has a high level of importance for improving the coating adhesion and deposition during spraying. In this experiment, grit blasting was used for preparing the composite substrates. More than 30 samples were grit-blasted for finding an optimized set of parameters for each type of composite substrates. These substrates include the typical composite substrate (without addition of any metallic mesh), the composite was fabricated by addition of a 200 steel mesh cloth (hereafter will be called as 200 mesh substrate), and the composite was fabricated by addition of a 400 steel mesh cloth (hereafter will be called as 400 mesh substrate). Table 2.2 shows the parameters and conditions in which these composite substrates were grit-blasted. The distance between the nozzle and substrate as well angle of grit impact were constant and 6 cm and 90 degree, respectively, in whole the process. The alumina grit used in the experiment had a diameter of about 80 μm. The variable grit blasting parameters in this experiment were the compressed air pressure and duration of grit blasting. Following the grit blasting, the surface of the samples was examined under a confocal microscope for analyzing the surface topography and roughness.

Table 2.2: Grit blasting parameters used for roughening the samples.

Sample No	Mesh count	Pressure (psi)	Time (s)	Standoff distance (cm)
1	No Mesh	60	150	6
2	No Mesh	68	120	6
3	No Mesh	76	120	6
4	No Mesh	76	150	6
5	No Mesh	90	120	6
6	No Mesh	90	150	6
7	No Mesh	90	180	6
8	200	60	90	6
9	200	60	120	6
10	200	60	150	6
11	200	70	140	6
12	200	70	170	6
13	200	76	70	6
14	200	76	105	6
15	200	76	130	6
16	200	76	150	6
17	200	76	200	6
18	200	86	130	6
19	400	50	240	6
20	400	60	100	6
21	400	60	150	6
22	400	60	180	6
23	400	60	180	6
24	400	66	180	6
25	400	70	120	6
26	400	70	133	6
27	400	70	140	6
28	400	76	110	6
29	400	76	130	6
30	400	76	130	6
31	400	76	150	6
32	400	80	60	6
33	400	80	120	6
34	400	86	130	6
35	400	90	38	6

2.3. Coating of Composite Substrates

Air Plasma Spray technique (APS) was used for the deposition of metallic coatings onto composite substrates. As depicted in Figure 1.12, a plasma torch comprises an anode, usually made of copper, as well as a cathode. An electrical arc is formed inside the torch by generation of an ignition between anode and cathode. The electrical arc ionizes and heats up the plasma gas injected at the base of the cathode, and then a high temperature and velocity plasma jet exits the torch. At the same time, the powder injected into the plasma jet, melt and reach to the substrate surface at a high velocity [30].

Table 2.3: Chemical composition and particle size distribution of the fine and coarse NiCrAlY Powders [51].

	Ni	Cr	Al	Y
Weight percentage	Bal.	21-23	9-11	0.9-1.2
Fine powder size distribution (μm)	–37 +11			
Coarse powder size distribution (μm)	-74 +45			

In this work, two types of NiCrAlY powders with different size distributions were utilized for spraying and fabrication of a heating element coating layer for the composite substrates. A 3MB plasma spray gun (Sulzer Metco, Westbury, NY) was also used to spray the NiCrAlY powders. The structure of this plasma spray torch is illustrated in Figure 2.5. In the first series of experiments, 1-by-1 inch substrates were coated using the NiCrAlY powder with the fine size distribution (Amdry 9624, Oerlikon Metco). The chemical composition and particle size distribution of this powder are presented in Table 2.3. As can be seen in Table 2.4, in this series, 5 experiments were done for finding a proper and nearly optimized set of spray parameters for the coating of the composite substrates using the fine powder. In the first experiment, reference parameters, provided by Oerlikon [52], were used for the spraying of NiCrAlY. In the second experiment, the electrical current was decreased from 500 A to 400 A. In the third and fifth

experiment, powder feed rate decreased from 64 g/min to 30 g/min and 48 g/min, respectively. In the fourth experiment, the stand of distance was increased from 13 cm to 15 cm. In each experiment, 1 stainless steel and 5 different composite samples were used as the substrates for the coating deposition process. The characteristics of these samples are shown in Table 2.5.

Table 2.4: The types of substrates used for the coating deposition process.

Experiment series	substrate type	Grit blasting condition		
		Pressure (psi)	Time (s)	Standoff distance (cm)
First Series	Typical composite	68	120	6
	200 mesh	Without grit blasting		
	200 mesh	76	150	6
	400 mesh	Without grit blasting		
	400 mesh	60	180	6
	Stainless steel	90	180	6
Second series	200 mesh	76	150	6
	400 mesh	60	180	6

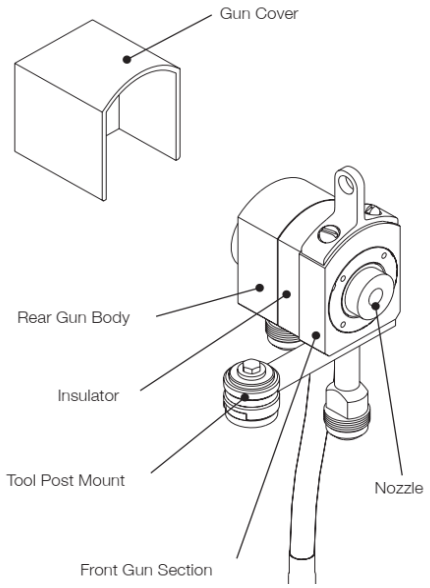

Figure 2.5: The structure of a 3MB plasma spray gun [52].

In the second series of experiments, composite substrates were coated using the coarse NiCrAlY powder (Amdry 9624, Oerlikon Metco). Table 2.3 depicts the chemical deposition and

particle size distribution of this powder. In this series, samples were first coated using the reference parameters. In the rest of experiments, the samples were coated with similar spray parameters to experiment 2 but with the different number of passes (see Table 2.5).The characteristics of the samples used in this series of experiments are shown in Table 2.4.

Table 2.5: The plasma spray parameters used for the coating of composite substrates

	Current (A)	Voltage (V)	Primary gas, Ar (l/min)	Secondary gas, H2 (l/min)	Powder feed rate (g/min)	Spray distance (cm)	Robot speed (m/s)	Number of passes
	First Series (fine NiCrAlY powder)							
Exp 1 (Ref)	500	60	43.8	6.57	64	13	1	10
Exp 2	400	60	43.8	6.57	64	13	1	10
Exp 3	500	60	43.8	6.57	32	13	1	20
Exp 4	500	60	43.8	6.57	64	15	1	10
Exp 5	500	60	43.8	6.57	48	13	1	15
	Second Series (Coarse NiCrAlY powder)							
Exp 6 (Ref)	500	60	43.8	6.57	64	13	1	4
Exp 7	400	60	43.8	6.57	64	13	1	3
Exp 8	400	60	43.8	6.57	64	13	1	4
Exp 9	400	60	43.8	6.57	64	13	1	5

Figure 2.6 shows the equipment used for the spraying of the composite substrate. Given that the composite substrates were vulnerable to the high-temperature gases and impact of high-temperature particles, they were cooled down using two air amplifiers and two air blowers to keep the substrates surface temperature as low as possible and below the composite maximum service temperature (about 120 °C) during spraying (see Figure 2.6). An infrared camera was also used for monitoring the substrates surface temperature during spraying.

After analyzing the coated samples, and finding the proper set of spray parameters and the appropriate powder type, more composite samples with larger dimensions (1-by-4 inch), were

prepared and coated for doing the electrical, thermal, and mechanical tests. Figure 2.7 shows the image of a grit-blasted 200 mesh sample after the coating deposition process.

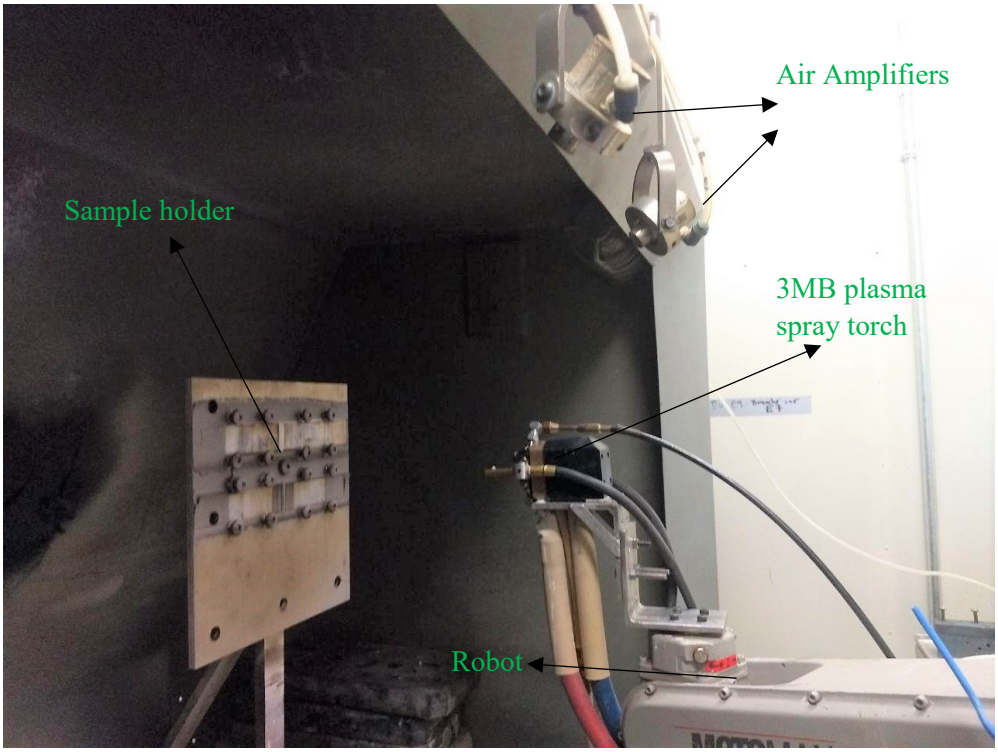

Figure 2.6: Plasma spray process equipment.

Figure 2.7: a grit-blasted 200 mesh sample after coating.

2.4. Characterization

On the completion of coating the composite substrates using the plasma spray process, the metallographic technique was used for analyzing the microstructure of the coated samples. Preparation of samples for characterization was made of four main steps: sectioning, mounting,

grinding, and polishing. In the first step, coated samples were cut and sectioned into smaller samples (0.5-by-1 inches) using a cutter machine. To facilitate analyzing the samples and to protect the samples during metallographic preparation steps, the samples were mounted using the cold mounting method. Epoxy and hardener were mixed together with the ratios of 89% and 11%, respectively. The mixture then was poured in the sample cap. After 24 hours, all the sample caps were put in an oven (about 1 hour) for better solidifying and curing. Once the mounting was completed, the mounted samples were ground by using abrasive papers. Doing an accurate and proper grinding is very important for minimizing the mechanical surface damages. In fact, grinding eliminates the uneven and damaged surfaces caused by cutting and sectioning the samples. The samples were ground with180, 300, and 600 mesh silicon-carbide (SiC) abrasive papers, rotated by a polishing machine, sequentially starting from the coarsest one to the finest one. The samples were ground using each abrasive paper for about two minutes. On completion of grinding, samples were washed by water for removing any residue and prepared for polishing. The main aim of polishing is to achieve a scratch-free, flat, and mirror-like surface. In this step, first, three splashes of diamond suspension with the particle size of 6 μm were applied to a rotating disk equipped with a hard cloth disk that was moisturized with lubricant. Samples were polished using this 6 μm diamond suspension for about two minutes. The same process then was repeated with another diamond suspension with the particle size of 3 μm. After this, the samples were cleaned using ethanol for examining under an optical microscope.

2.5. Electrical Characterization

Given that the amount of heat generated by a heating element (de-icing element) coating for a given current depends directly on the coating electrical resistance, determining the electrical properties of the coatings has a high level of importance.

Electrical resistivity is a property of a material indicating how strongly that material opposes and resists the electrical current flow [53].It should also be noted that resistivity is an intrinsic property and independent of the shape and size of the specimen. The relation between the resistance and resistivity of a specimen can be written by the following equation:

$$R = \rho \frac{l}{A} = \rho \frac{l}{bd} \quad \textbf{(1)}$$

In which,

R is the electrical resistance (**Ω**)

ρ is the resistivity (**Ω**.m)

l is the specimen length (m)

A is the specimen cross-section area (m^2)

b is the specimen width (m)

d is the specimen thickness (m)

Sheet resistance is another electrical term used more for electrical characterizing the relatively thin coatings and paints .By referring to Equation 1, the sheet resistance can be calculated as follow:

$$R = \rho \frac{l}{A} = \rho \frac{l}{bd} = \frac{\rho}{d} \frac{l}{b} = R_S \frac{l}{b} \quad \textbf{(2)}$$

Where

$$R_S = \frac{\rho}{d} \quad \textbf{(3)}$$

In which, R_s is the sheet resistance. The sheet resistance is the resistivity of a specimen divided by its thickness. The units of Eq. 3 resolves to **Ω**. However, since sheet resistance, in fact, represents and shows the resistance of a square regardless of its dimension, **Ω**/□ or

Ω/square units are more common and representative. More details about sheet resistance are discussed in the result and discussion chapter.

In this experiment, the four-point electrical probe technique was used for determining the electrical properties of the specimens. This technique is very useful for eliminating the wire and contact resistances that may cause an error in calculating the resistance of the sample [54]. A schematic of this method is shown in Figure 2.8. As can be seen in this figure, for doing the four point probe test, four wires were attached to the samples top face. A constant current was applied to the sample through probes 1 and 4 connected to a power supply. In addition, an ammeter was installed in series with the circuit and between the power supply and probe 4 for increasing the accuracy of the current measurement. A voltmeter was connected to the sample using probes 2 and 3 for measuring the voltage drop between these two locations. It should also be noted, given that the voltmeter is parallel to the circuit and has a very high resistance, no current passes through the voltmeter, so it has no impact on the amount of current registered on the ohmmeter. Different electrical currents (6, 9, and 12 A) were applied to the samples, and the resultant voltage drop between locations 2 and 3 was measured using a voltmeter at the same time. After that, the V-I graph was drawn for each coated sample, and the resistance was calculated using $R_{2-3} = \frac{V}{I} = \frac{\Delta V}{\Delta I}$ formula. Once the resistance was found, the resistivity was calculated using $\rho = R\frac{A}{l_{2-3}}$ formula.

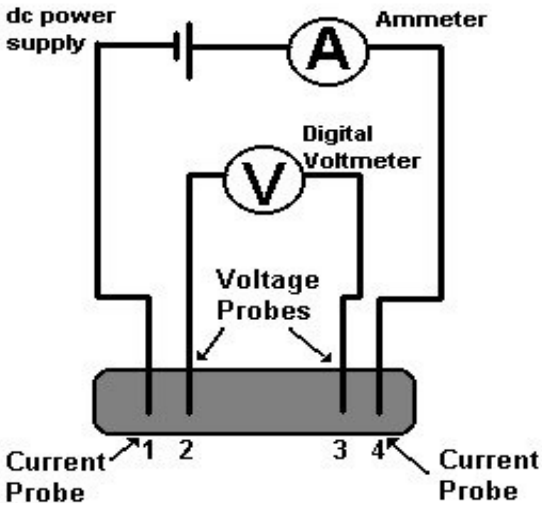

Figure 2.8: 4 point probe method schematic [54].

2.6. Surface Temperature Measurement

In this step, the surface temperature of the coated samples was measured at the ambient temperature and under free convection condition. Three thermocouples type k (KMQSS-062U-36, Omega, Canada) were attached to the surface of the coated samples to measure the temperature along the coating surface and to make sure about the surface temperature uniformity while the samples were connected to a power supply. The surface temperature was recorded for each coated sample for 3 different applied currents, 6, 9, and 12 A. In addition to the thermocouples, an infrared camera was used for monitoring the surface temperature and its uniformity. Each temperature measurement was repeated for 3 times for ensuring about the reliably of the results. The power generated by each sample was also calculated by $P = VI = RI^2$. After recording the temperature, a temperature profile was drawn for each coated sample.

2.7. Adhesion Strength Test

In this step, flatwise tensile test was performed for measuring the adhesion strength (bond strength) of the coated samples. For this purpose, first, a two-component adhesive (Henkel Loctite Hysol EA 9392 AERO Epoxy Adhesive Gray, LOCTITE, Henkel Canada Corporation, Canada) including epoxy and hardener were mixed together with a weight ratio by weight of 100: 32. On completion of the mixing, a thin and even layer of the mixture was applied on both sides of the 1-by-1 inch coated samples. Following this, as can be seen in Figure 2.9a, the samples were sandwiched between two stainless steel blocks, and two metal pieces were used for aligning the sample and blocks. Samples and blocks were then put in an oven at the temperature of 85 ^{o}C and for about 90 minutes for curing the adhesive. Once the curing process was completed, the blocks were connected to two Wyoming flatwise tensile test fixtures by using two pins (see Figure 2.9b), and they were placed in a flatwise tensile machine (with the displacement rate of 0.50 mm/min) for applying tension and measuring the adhesion strength of the coatings. The samples then were analyzed for detecting the failure type. The details will be discussed in the next chapter.

For removing the adhesive and samples from the stainless steel blocks, they were placed in an oven with the temperature of 250 °C for about 60 minutes so that the adhesive was removed easily by scraping the steel block cross-section.

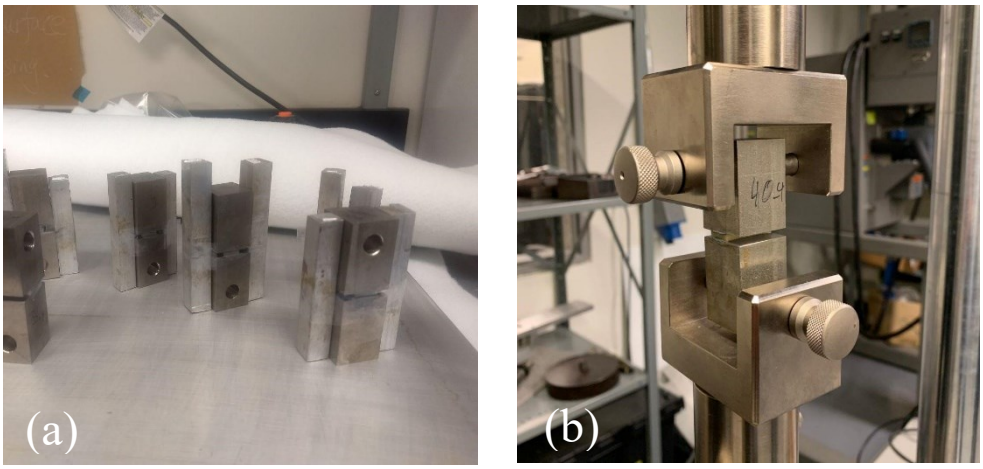

Figure 2.9: Flatwise tensile test (a) sample alignment, (b) test equipment.

Chapter 3: Results & Discussion

3. Results and Discussion

As it was mentioned in the previous chapter, three types of composite substrates were prepared for the deposition of NiCrAlY coating, which are: 1) composite plate with a woven stainless steel wire cloth 400 mesh as the top layer, 2) composite plate with a woven stainless steel wire cloth 200 mesh as the top layer, and 3) typical composite plate without using any metallic mesh. Stainless steel mesh cloth was used in the first two plates for two important aims. Firstly, to protect the composite fibers from the impact of high velocity and high-temperature particles. Secondly, to improve the coating adhesion strength as composite materials have low surface free energy and deposition of a metallic coating layer with high adhesion strength is difficult. As can be seen from Table 3.1 epoxy has a surface free energy of 43 dynes/cm while this value is in the range of 700-1100 dynes/cm for stainless steel [55].

Table 3.1: Surface free energy of different materials [55]

Substrates	Surface Energy (Dynes/cm)	
Copper	1103	Highest bonding strength
Aluminum	840	
Zinc	753	
Stainless Steel	700-1100	
Tin	526	
Lead	458	
Glass	250-500	
Kapton® (Polymide)	50	
Phenolic	47	
Nylon	46	
Alkyd Enamel	45	
Polyester	43	
Epoxy	43	
Polyurethane Paint	43	
ABS	42	
Polycarbonate	42	
PVC (Polyvinyl Chloride)	39	
Noryl®	38	
Acrylic	38	
Polane® Paint	38	
PVA	37	
Polystyrene	36	
Acetal	36	
EVA	33	
Polyethylene	31	
Polypropylene	29	
Tedlar®	28	
Silicones	22-24	
Teflon®	18	Lowest bonding strength

3.1. Analysis of the Composite Substrate Structure before Coating Process

Before grit blasting and preparing the substrates for the coating deposition process, the composite substrates were characterized, and their cross-sections were examined under an optical microscope. Figure 3.1 shows the low and high magnification microscopic images of 200 mesh substrate cross-section after fabrication. As can be seen in this figure, the resin has penetrated perfectly through the stainless steel mesh and has formed a very thin and uniform layer on top of the steel mesh. The cross-section of 400 mesh substrate is shown in Figure 3.2. It can be seen that the overall resin penetration through the steel mesh is relatively good. However, in some locations, as shown in Figure 3.2b, the resin penetration is not sufficient and good enough. This is because the steel mesh used in the 400 mesh substrate is very fine, and consequently a perfect resin penetration through the steel mesh is very difficult and demands to apply high pressures to the composite plates during the curing process. By comparing Figure 3.1b and Figure 3.2b, it can be concluded that the steel mesh in the 200 mesh substrate has a better bonding and condition.

Once the analysis of the composite substrates cross-section was completed, the samples were grit-blasted with different parameters provided in Table 2.2. Grit blasting and proper preparing of the polymeric samples prior to the coating are important for the fabrication of a uniform coating with high quality. So, for finding the best and optimized preparing condition, many composite samples were grit-blasted with different parameters, and their surface was examined under a confocal microscope. The analysis of microscopic images of a number of samples is presented in this section.

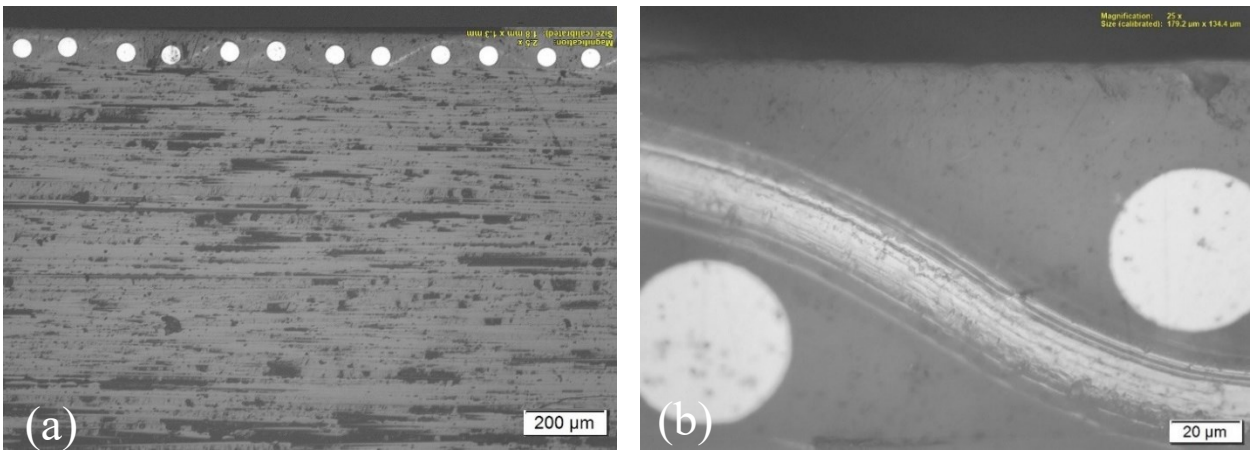

Figure 3.1: 200 mesh substrate cross section with the magnification of (a) 5x, and (b) 50 x.

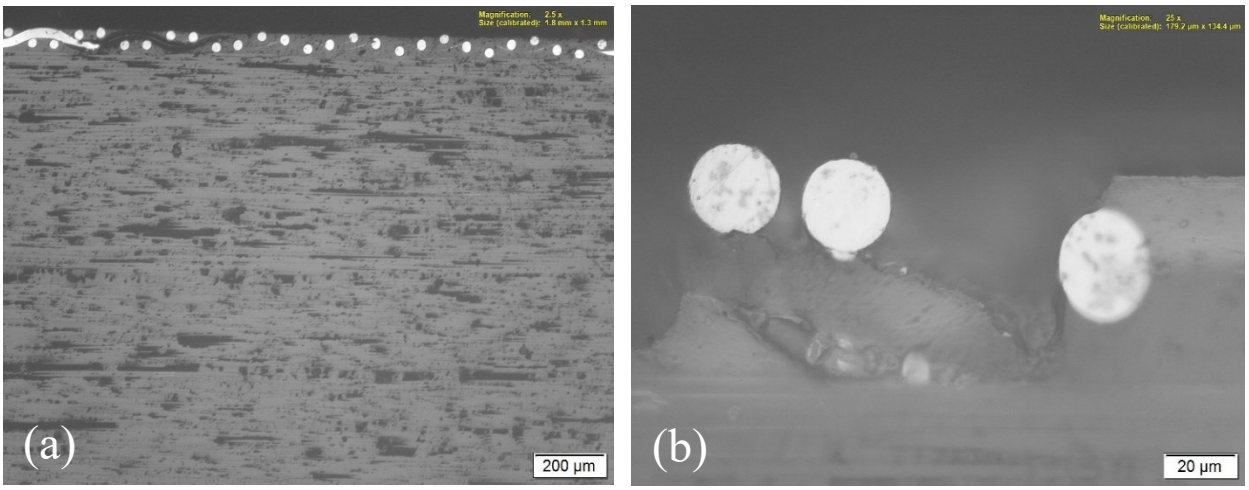

Figure 3.2: 400 mesh substrate cross section with the magnification of (a) 5x, and (b) 50 x.

3.2. Preparation of the composite substrates

As shown in Table 2.2, seven typical samples (without mesh) were grit-blasted with different parameters. In all samples, a lot of fibers were removed from the top of the composite substrates. This is due to the fact that polymeric materials are typically very vulnerable, and the impact of high-velocity grit particles can easily damage and remove the top-layer fibers.

The confocal images of the surface of a 200 mesh substrate grit-blasted with a pressure of 76 psi and for 200 seconds are shown in Figure 3.3. It can be seen in this figure that a few steel mesh wires have been removed or damaged due to grit blasting (shown by the red circles). So, to prevent inducing damage to the steel mesh cloth wire, a number of 200 mesh substrates were grit-blasted with lower pressures for a shorter period of time. For example, the confocal images of a 200 mesh substrate grit-blasted with the pressure of 50 psi for 90 s are shown in Figure 3.4. In this sample, unlike the previous case, no damage is induced to the steel wires. However, in this case, a high percentage of the wires is still covered with epoxy, and this may have a negative impact on coating adhesion in the next steps due to the fact that the more the steel wires there are on the substrate surface, the better the coating adhesion will be. Finally, to approach to an ideal and optimized state, other 200 mesh substrates were grit-blasted with higher pressures and for a longer amount of time. It was found that the best result might be achieved by grit blasting the 200 mesh substrate with the pressure of 76 psi for 150 s. As depicted in Figure 3.5, in this case, steel wires are in good

form, and the epoxy is removed from the top of the wires perfectly, which makes it ideal and adequate for the coating deposition.

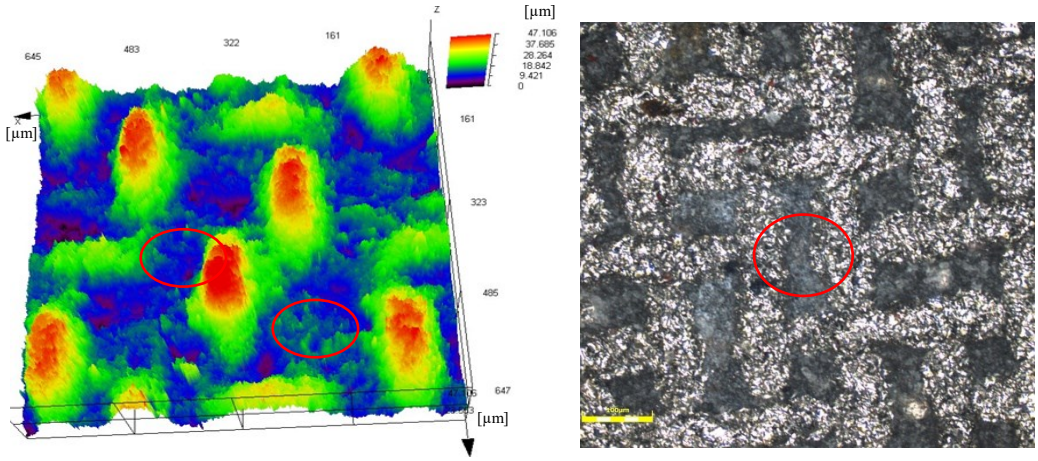

Figure 3.3: Confocal images of a grit-blasted 200 mesh substrate (P= 76 psi and t= 200 s).

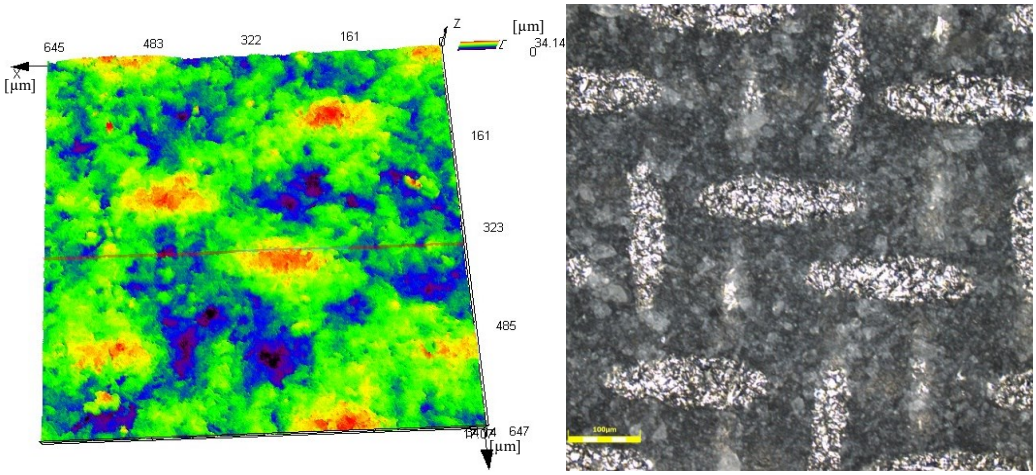

Figure 3.4: Confocal images of a grit-blasted 200 mesh substrate (P= 50 psi and t= 90 s).

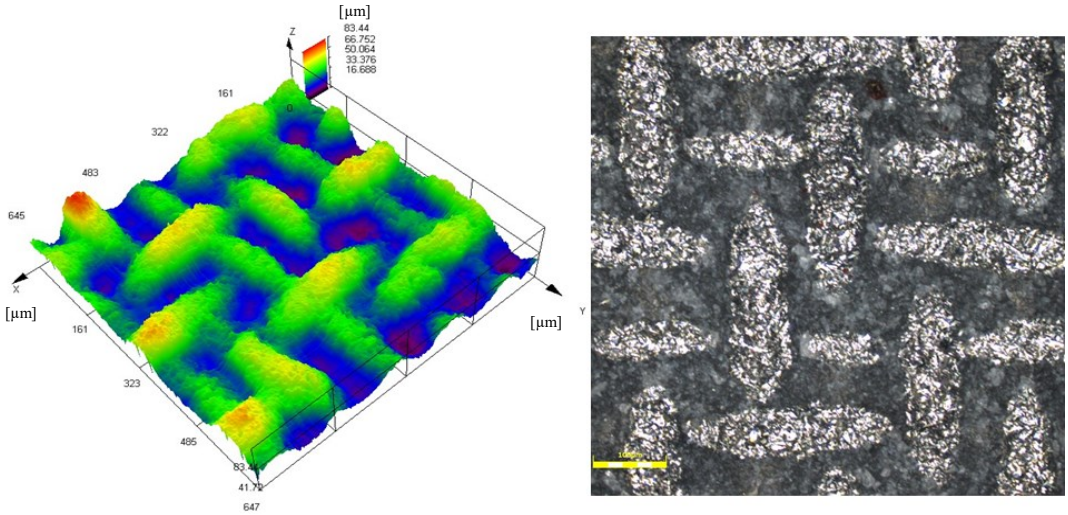

Figure 3.5: Confocal images of a grit-blasted 200 mesh substrate (P= 76 psi and t= 150 s).

To find an optimized and proper set of parameters for grit blasting the 400 mesh substrates, a few 400 mesh substrates were grit-blasted with the optimized parameters achieved for grit blasting the 200 mesh substrates (P= 76 psi and t= 150 s). However, in this case, as shown in Figure 3.6, a lot of steel wires were removed from the substrate surface, and even significant damages were induced to the composite part of the substrate. A possible explanation for this might be that 400 mesh cloth wires are thinner and consequently more vulnerable to the impact of grit particles in comparison to the 200 mesh cloth wires. Following this, some other 400 mesh substrates were grit-blasted with relatively low pressures and for a short amount of time. For example, the confocal images of the surface of a 400 mesh substrate grit-blasted with the pressure of 60 psi for 80 s are shown in Figure 3.7. It is apparent that the grit blasting pressure and time had not been sufficient as there is still a lot of epoxy on top of the still wires. Finally, for finding a proper set of parameter, other 400 mesh substrates were grit-blasted with the pressures between those of the previous cases for different amounts of time. The best results were achieved once the 400 mesh substrates were grit-blasted with the pressures around 60 psi for about 180 s. As shown in Figure 3.8, the steel wires are undamaged and in good condition, however, in this case, a few steel wires are still covered with the epoxy materials.

Globally, by comparing Figure 3.3 to Figure 3.8, it can be found that optimizing the grit blasting parameters is critical for roughening the substrate surface. The 200 mesh substrates are less sensitive and vulnerable to the grit blasting parameters as their cloth steel wires are thicker and more resistant to the impact of high-velocity particles, and better results were obtained by grit blasting this kind of substrate, compared to the grit-blasted 400 mesh substrates. Furthermore, as the metallic mesh holes dimensions were smaller than the grit blasting sand diameter, the sand could not penetrate to the composite part of the substrates and break the fibers during grit blasting. By measuring the surface roughness, it was also found that the 400 mesh substrate grit-blasted with the optimized parameters has a surface roughness about 7 μm, while this value for the 200 mesh grit-blasted with the optimized parameter is about 11 μm (about 50% higher compared to the grit-blasted 400 mesh substrate). This might be due to the relatively large voids existing on the 200 mesh substrate surface. So, it is expected that using this kind of substrate results in a better coating deposition and adhesion during spraying. Once the samples were grit-blasted, they were cleaned using compressed air and acetone, and then prepared for the coating deposition process.

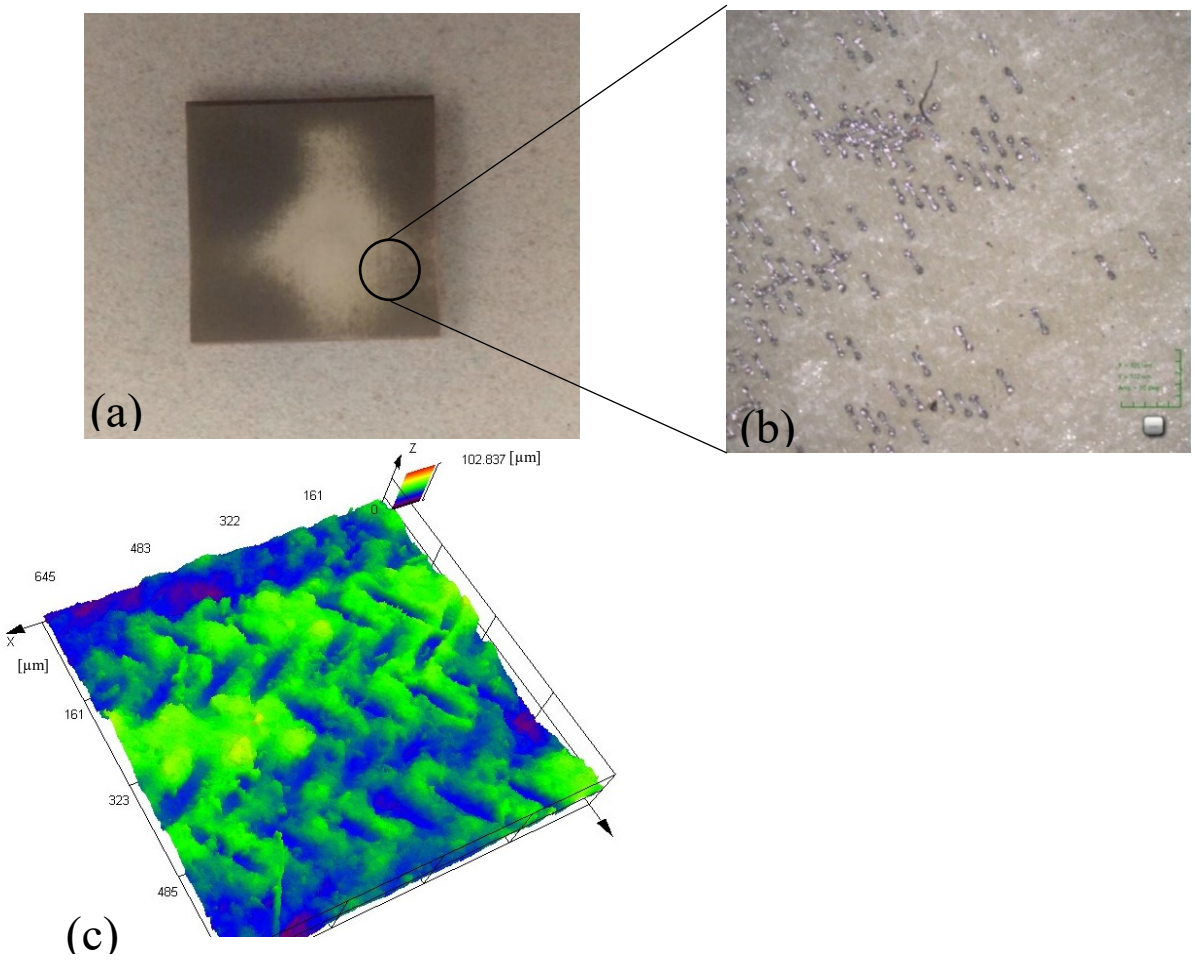

Figure 3.6: Images of the surface a 400 mesh substrate grit-blasted with P=76 psi and t=90 s, (a) typical picture, (b) microscopic picture, and (c) confocal image.

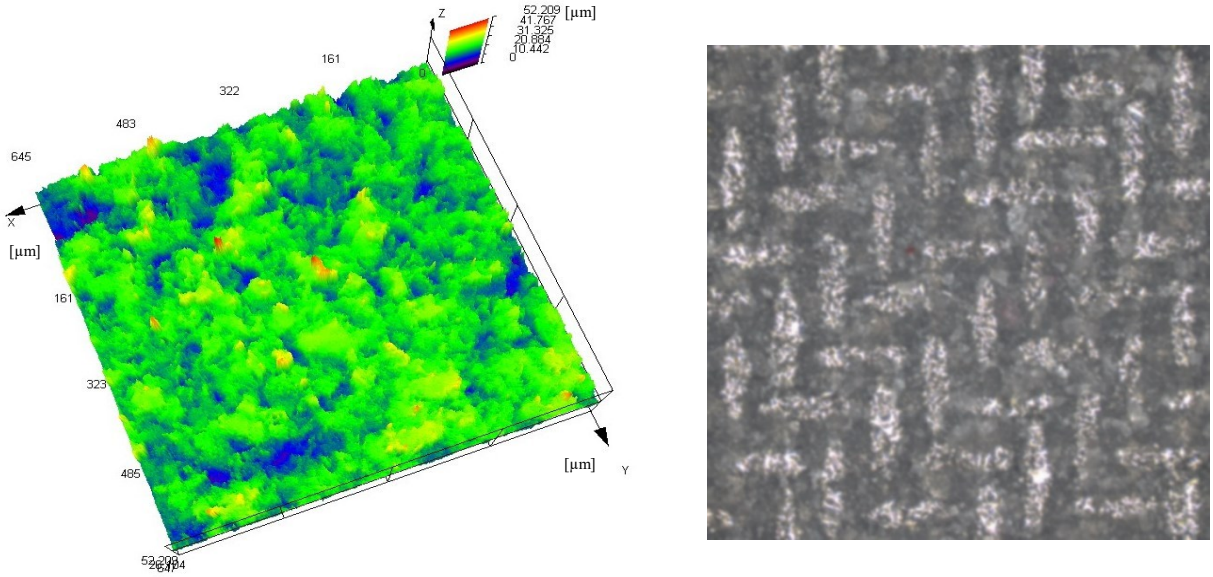

Figure 3.7: Confocal image of a 400 mesh substrate grit-blasted with P=60 psi and t=80 s.

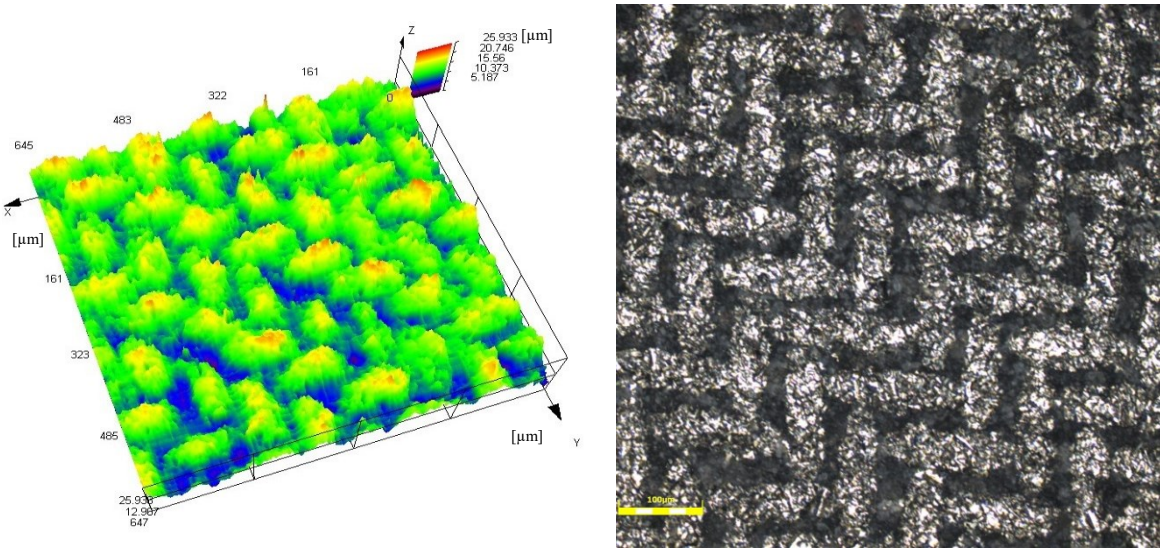

Figure 3.8: Confocal image of a 400 mesh substrate grit-blasted with P=66 psi and t=180 s.

3.3. Coating of Composite Substrates Using Plasma Spraying

3.3.1 Coating of the composite substrates using the fine NiCrAlY powder

As discussed in section 2.3, in the first series of experiments, 5 experiments were done for finding a decent and relatively optimized set of parameters for depositing a NiCrAlY coating layer onto composite substrates. In this series of experiments, the NiCrAlY powder with the fine size distribution (–37 +11 µm) was used as the coating material. In each experiment, only one spraying parameter was changed for analyzing the effects of the spray process on the coating microstructure, quality, and adhesion. The properties of the substrates used in this series of experiments are presented in Table 2.4

In experiment 1, samples were coated using the reference parameters. As shown in Figure 3.9, in this experiment, all the composite samples were burnt, and in the cases of 200 and 400 mesh substrates, in addition to the burning, the steel cloth and coating were peeled off from the composite part of the substrate. These results might be explained by the fact that the temperature of the substrate during coating deposition (about 200 °C) exceeded its glass transient (90 °C) and curing temperatures (120 °C) for a long amount of time. When the temperature goes over the

glass transient temperature, the composite starts transiting from a hard and glassy state into a soft and rubbery state. Consequently, the bonding between the steel wire and the composite part gets loose and the steel mesh cloth starts debonding from the substrate. Furthermore, once the temperature gets higher than the composite curing temperature, the composite epoxy starts burning.

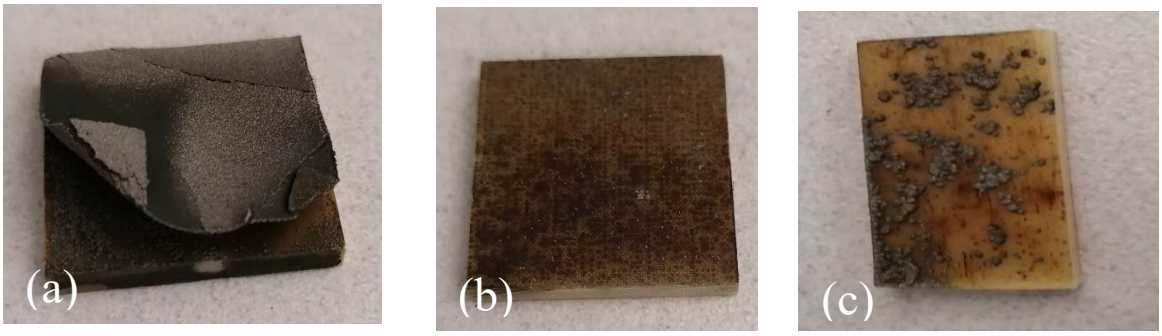

Figure 3.9: Burnt composite substrates after coating with experiment 1 spray parameters, (a) grit-blasted 200 mesh substrate, (b) 200 mesh substrate without grit blasting, and (c) typical composite substrate.

In experiment 2, the plasma current was decreased from 500 A to 400 A. Indeed, in this experiment, the input power was lessened about 25% compared to the first experiment. The maximum surface temperature of the substrates during spraying was about 105 °C. Figure 3.10 shows the cross-section of the samples coated using second experiment parameters. It can be seen from Figure 3.10a when a typical composite is used as substrate without any metallic mesh, the coating deposition efficiency is very low and in, the most parts of the composite surface, there is no coating. As explained earlier, this low deposition is due to the low surface energy and high chemical inertness of the polymeric materials [17]. In addition, in the region shown by a red circle, it can be seen that the composite surface is not uniform as a lot of fibers are removed from top of the composite due to the grit blasting done prior to the spraying process. Figure 3.10b and c show the cross-section of not grit-blasted 200 and 400 mesh substrates after coating. From these figures, it is apparent that in these cases, the coating deposition is better than the typical composite, but it is still non-uniform and limited. The main reason for this limited deposition, as mentioned earlier, is that a thin layer of epoxy has covered the metallic mesh (see Figure 3.1and Figure 3.2), so when the molten particles reach to the substrate surface, they face with a polymeric surface instead of a metallic one. In addition, since these two samples were not grit-blasted before the coating deposition stage, there was no rough surface for the molten particles to lock into and fully adhere [56]. However, in these cases, unlike the previous substrate, fibers are

undamaged and in good condition. Figure 3.10d and e show the cross-section of a grit-blasted 200 mesh substrate after coating at low and high magnification, respectively. From these images, it can be found that the coating was deposited with high uniformity and quality, and without inducing any damages to the composite fibers. In fact, in this type of substrate, the steel mesh protects the composite part, especially the fibers, from the impact of high-velocity particles, and given that the composite surface is dominated with the steel wires, the coating is deposited with high uniformity and efficiency. In addition, the holes created by grit blasting between the steel wires are expected to have an important influence on improving the anchorage of the molten particles to the substrate surface, and consequently on improving the coating adhesion. As shown in Figure 3.10f and g, in the case of grit-blasted 400 mesh substrate, similar to the girt-blasted 200 mesh substrate, the coating was deposited with high uniformity and efficiency. Finally, Figure 3.10h shows the cross-section of a coated stainless-steel sample. In this case, the coating is very similar to those of the grit-blasted 200 and 400 mesh substrates from thickness, uniformity, and quality points of view. Indeed, by comparing Figure 3.10d-h, it can be found that by considering the stainless steel block as a reference sample, the deposition efficiency of the coating on 200 and 400 mesh substrates is similar.

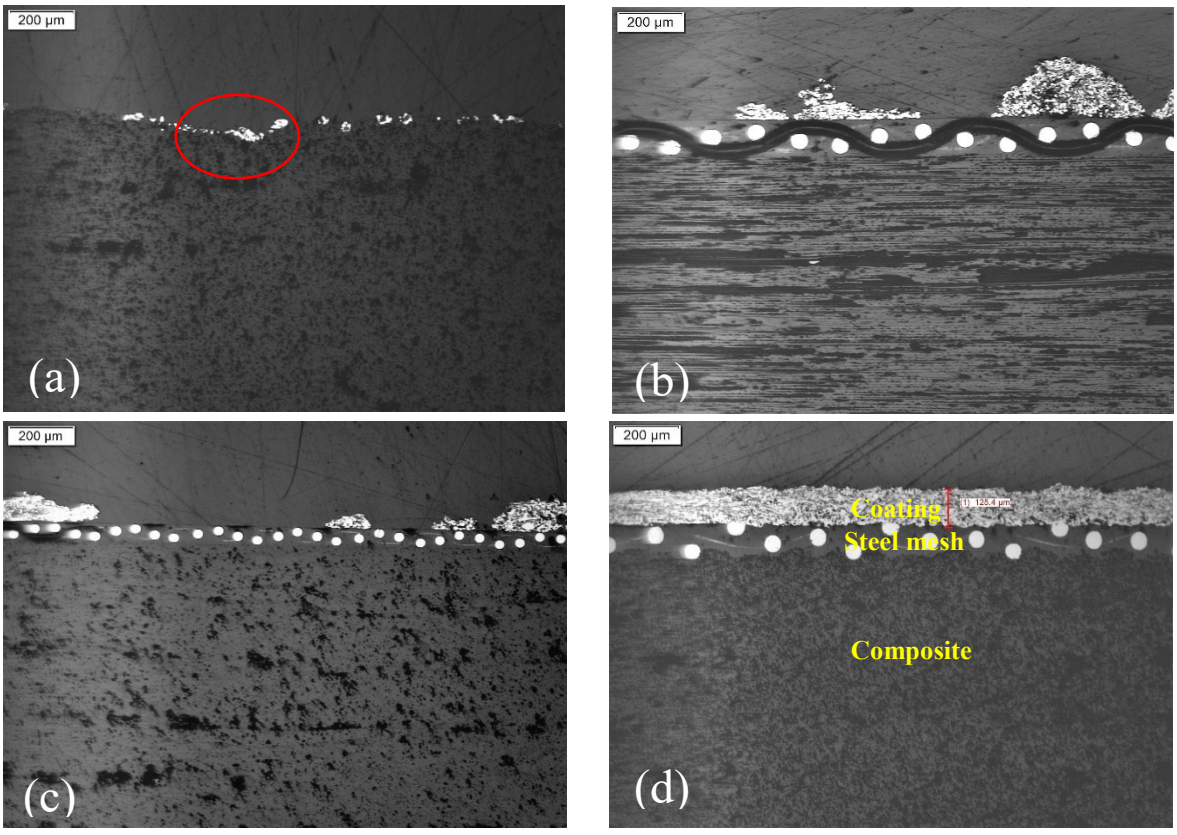

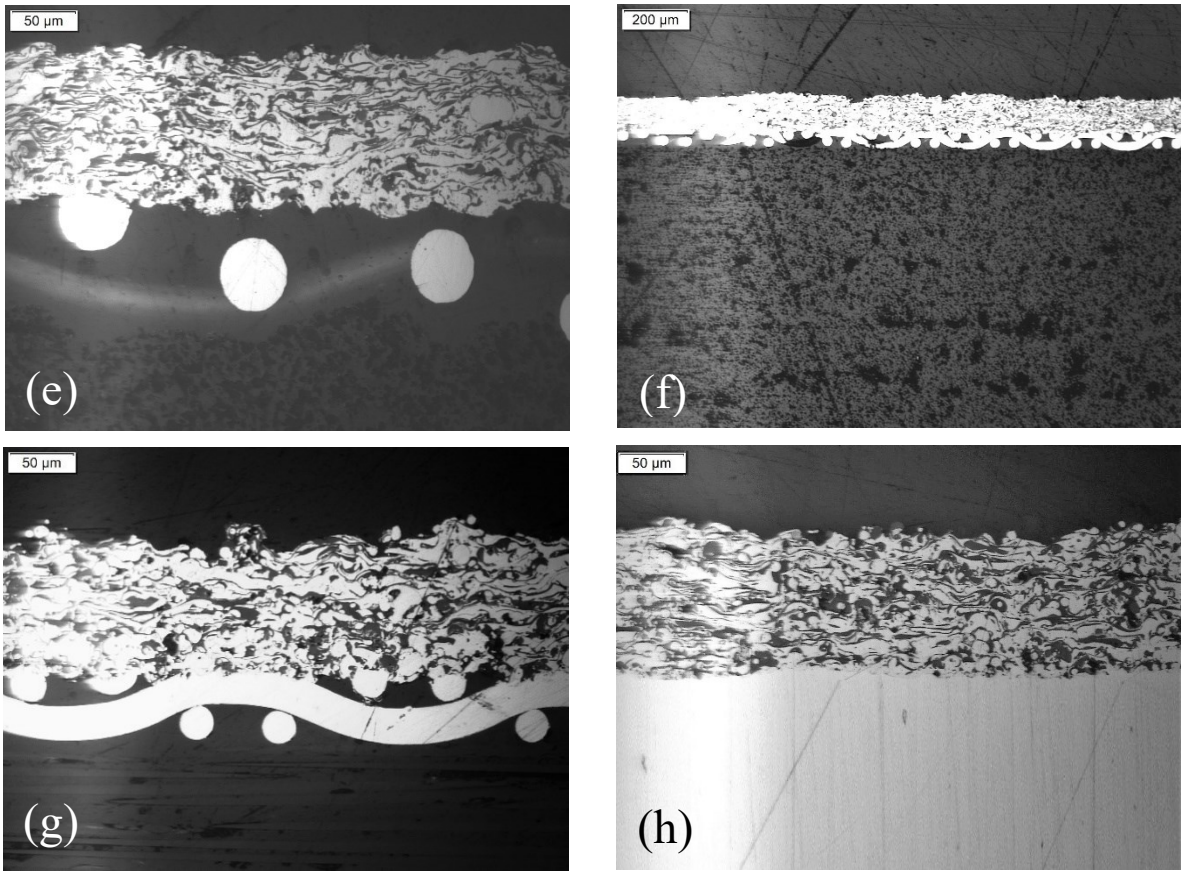

Figure 3.10: Experiment 2, cross section of (a) grit-blasted typical composite, (b) 200 mesh substrate without grit blasting, (c) 400 mesh substrate without grit blasting, (d) grit-blasted 200 mesh with low magnification, (e) grit-blasted 200 mesh with high magnification, (f) grit-blasted 400 mesh with low magnification, (g) grit-blasted 400 mesh with high magnification, and (h) grit-blasted stainless-steel sample after coating.

In experiment 3, the powder feed rate was decreased from 64 to 30 g/min. In this experiment, unlike the first experiment, the samples were not burnt; however, the coating deposition efficiency was low. As can be seen in Figure 3.11, even in the grit-blasted 200 and 400 mesh substrates, the coating deposition is very limited, non-uniform, and inadequate. The maximum surface temperature of the substrates in this experiment was about 110 °C.

In experiment 4, the standoff distance was increased from 13 cm to 15 cm. In this experiment, similar to the previous one, the coating deposition was low and limited. A possible explanation for this might be that at relatively large standoff distances, the re-solidification of partially molten particles contributes to an increment in the coating porosity, and since the coating porosity has an inverse relationship with deposition efficiency, the larger standoff distances

result in lower deposition efficiencies [13]. In addition, partial burnings were observed in all the composite samples. The maximum surface temperature of the substrates during spraying was about 165 °C.

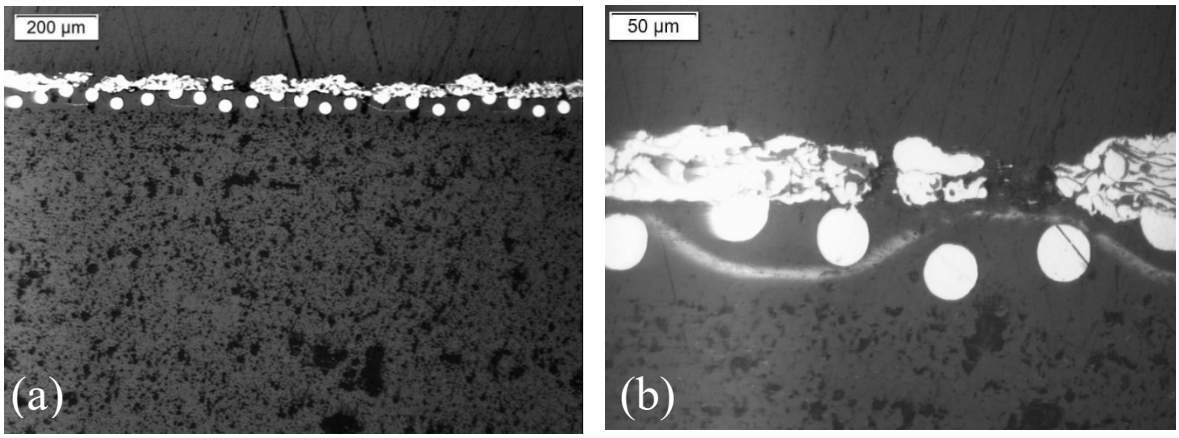

Figure 3.11: Experiment 3, cross-section of a grit-blasted 400 mesh substrate after coating process with (a) low magnification, and (b) high magnification.

In experiment 5, the powder feed rate was decreased from 64 to 48 g/min. In this experiment, similar to experiment 2, successful coating deposition on the grit-blasted 200 and 400 mesh substrates was observed (see Figure 3.12). However, in the case of 400 mesh substrate, since the steel wires were thinner and weaker compared to the 200 mesh cloth wires, and as mentioned earlier, due to imperfect bonding of the steel mesh cloth to the composite part, in some cases the steel cloth and coating were peeled off slightly from the corners of the composite part during spraying. In fact, in this experiment, the substrates surface temperature, during spraying, was higher compared to that of experiment 2 but lower compared to those of experiments 1 and 4. In the other samples, the coating deposition efficiency was low and insufficient. The maximum surface temperature of the samples during spraying was about 150 °C.

By comparing Figure 3.9 to Figure 3.12, it can be found that the best results for the deposition of NiCrAlY powder with the size distribution of -37+11 µm were achieved by the coating of grit-blasted 200 mesh substrate using experiment 2 spray parameter. In this case, no damage was induced to the composite matrix and fibers, the coating and steel mesh cloth were not peeled off from the composite part, and the deposited coating had a very uniform thickness.

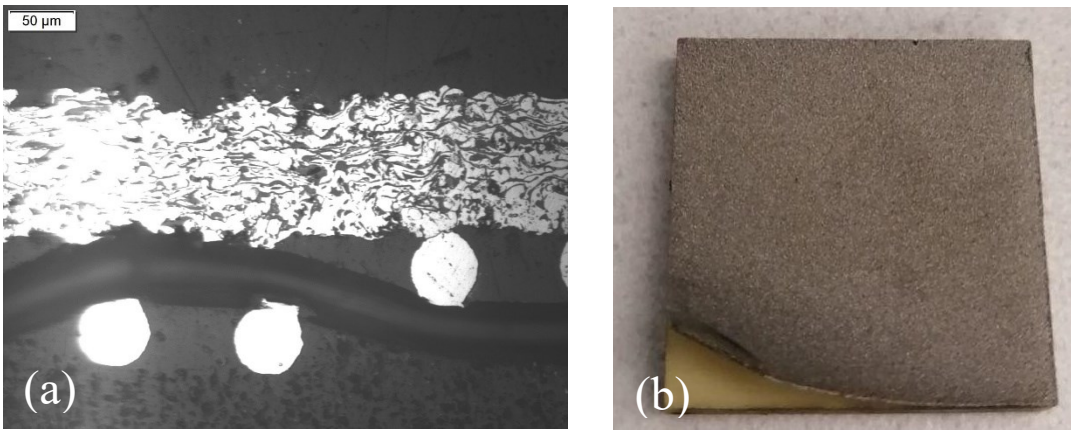

Figure 3.12: (a) Cross-section of a grit-blasted 200 mesh substrate, and (b) picture of grit-blasted 400 mesh substrate after coating deposition process, coated using experiment 5 spray parameters.

3.3.2. Coating of the composite substrates using the coarse NiCrAlY powder

In the second phase of experiments (experiments 6-9), composite substrates were coated using the coarse NiCrAlY powder (Amdry 9625) with the size distribution of -74+45 µm for making a comparison between the coatings sprayed using the coarse powder and those sprayed using the fine powder. This comparison mainly includes analyzing the coating microstructure, thickness, amount of oxidation, and electrical resistivity for determining which type of coating has abetter performance as a heating element. In this series of experiments, just grit-blasted 200 and 400 mesh substrates were used as the substrate as proper and acceptable results were achieved only by using these kinds of substrates in the previous phase experiments.

In experiment 6, similar to the first experiment, composite substrates were coated using the reference spray parameters. In this experiment, all the samples were burnt dramatically after the second pass of spraying. The samples burning was more severe in comparison to those of experiment 1. This might be explained by the fact that the powder used in this experiment has a volume about 15 times greater than that of the powder used in the first series of experiment. So, when the coarse powder is used as the coating material, the amount of heat transferred to the substrate locally by each molten particle is considerably higher, and this could contribute to more substrate damage and burning. The maximum surface temperatures of the samples in this experiment was about 215 °C.

Given that NiCrAlY coatings were successfully deposited onto both grit-blasted 200 and 400 mesh substrates using experiment 2 spray parameter, in the experiments 7-9, samples were coated with similar parameters but with different number of passes to see whether achieving an acceptable coating by using those parameters and coarse NiCrAlY powder is possible or not.

In experiment 7, samples were coated in three passes. In this experiment, unlike experiment 6, composite samples were not damaged and burnt after the spraying process. However, as shown in Figure 3.13, in the both grit-blasted 200 and 400 mesh substrates, the coating is not uniform at all. In fact, in some parts, the coating is very thin and has a thickness of about 10 µm while in the other parts, the coating is relatively thick and has a thickness of about 80 µm. The maximum surface temperature of the substrates during spraying was about 109 °C.

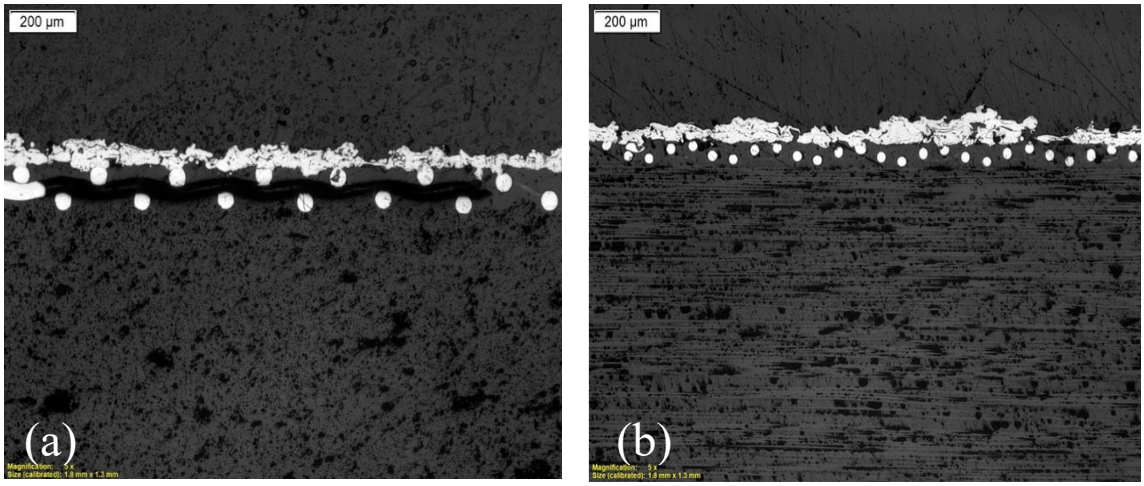

Figure 3.13: Cross-section of (a) grit-blasted 200 mesh substrate, and (b) grit-blasted 400 mesh substrate coated using experiment 7 spray parameters.

In experiment 8, the coating was deposited onto the composite samples in 4 passes. Figure 3.14 shows the cross-section of composite substrates coated in this experiment. It can be seen that on the contrary to experiment 7, the coating in both grit-blasted 200 and 400 mesh substrates has a relatively proper uniformity. In addition, the composite parts are undamaged and in good condition (without epoxy burning and fiber breakage). The average thickness of the deposited coatings is about 84 µm. By comparing Figure 3.10 and Figure 3.14, it can be found that the NiCrAlY coating deposited using Amdry 9625 (the powder with the size distribution of -74+45 µm) has a higher porosity and lower degree of oxidation in comparison to the one deposited using Amdry 9624 (the powder with the size distribution of -37+11 µm). The higher porosity

could be attributed to the fact that in the plasma plume, coarse particles have relatively lower melting efficiencies and lower speed than fine particles which result in larger amounts of unmolten particles and the formation of big pores between coating splats [57]. In addition, the total surface area of the fine particles (sum-up surface are of all particles) sprayed in a period of time is considerably greater than that of the coarse particles which contributes to more heat absorption, and consequently more oxidation when the fine powder is used for the coating deposition. The maximum surface temperature of the substrates in this experiment also was about 118 °C.

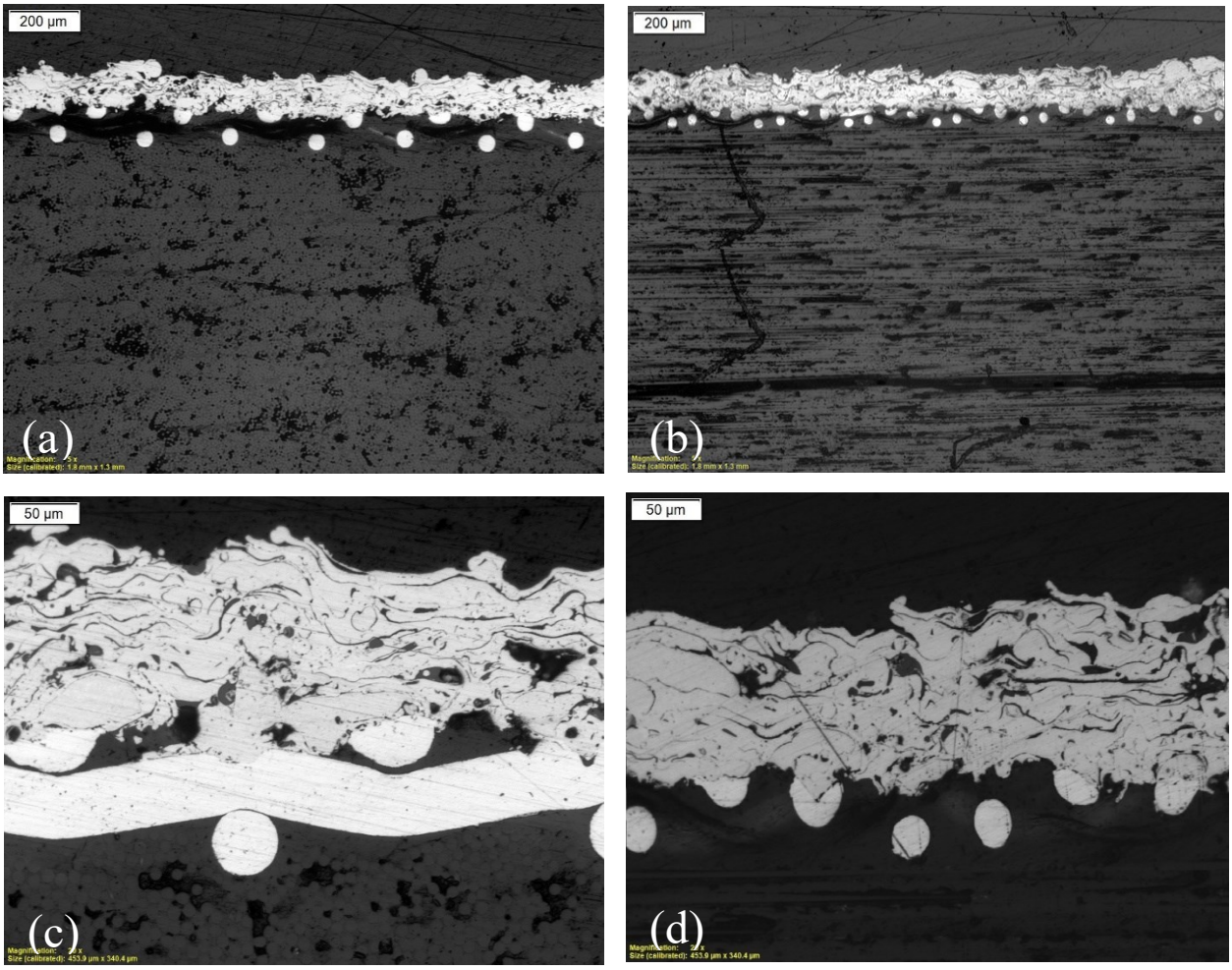

Figure 3.14: Cross-section of (a) girt-blasted 200 mesh substrate with low magnification, (b) girt-blasted 400 mesh substrate with low magnification, (c) girt-blasted 200 mesh substrate with high magnification, and (d) girt-blasted 400 mesh substrate with high magnification after coating by experiment 8 spray parameters.

Finally, in experiment 9, the coatings were sprayed onto the composite substrates in 5 passes. The coating was deposited on the top of grit-blasted 200 mesh substrate utterly and without inducing any damage to the composite part (see Figure 3.15). However, when the grit-blasted 400 mesh was used as a substrate, the coated steel mesh cloth started peeling off during the fifth pass. It seems possible that this peeling off was due to the imperfect bonding of the steel mesh cloth to the composite part, the weak and thin steel wires, as well as the stresses induced to the substrate by increasing the number of passes and coating thickness. The coatings deposited in this experiment had an average thickness of about 100 µm (20% higher than that of the previous experiment coatings). The substrates had a maximum surface temperature of about 135 °C

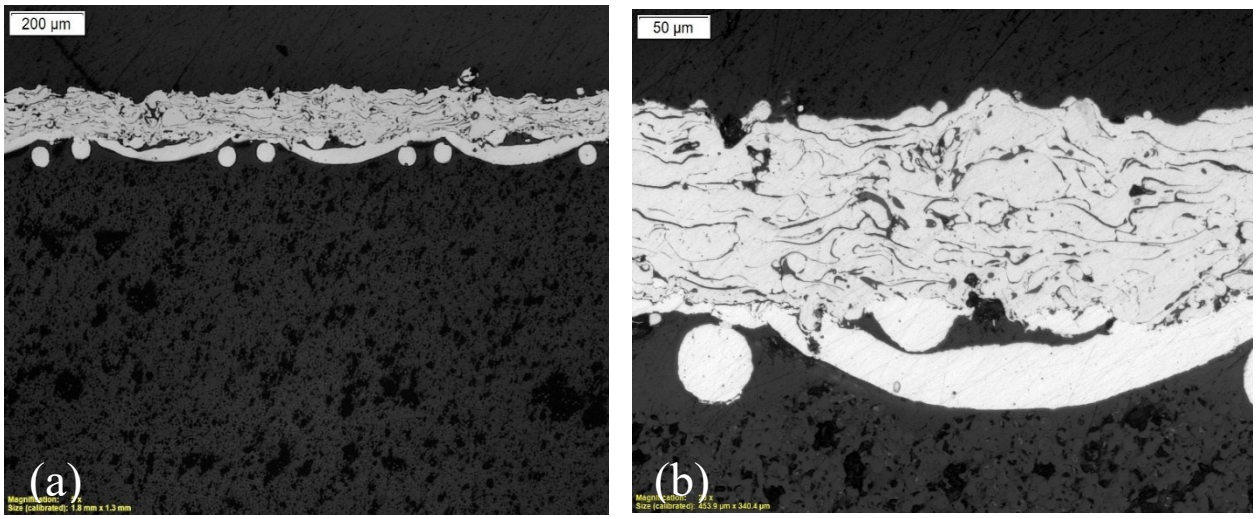

Figure 3.15: Cross-section of a grit-blasted 200 mesh substrate coated using experiment 9 spray parameters with, (a) low, and (b) high magnifications.

Overall, the results of these nine experiments show that an appropriate and uniform NiCrAlY coating layer could be deposited onto the grit-blasted 200 and 400 mesh substrates by using both fine and coarse NiCrAlY powders. It can also be seen that using the powder with the fine size distribution has resulted in the formation of a coating with more uniformity as the powder particles are significantly smaller compared to those of the coarse powder. The amount of oxidation is considerably higher in the coatings in which the fine powder was used as the coating material while the amount of porosity is higher in the coatings sprayed by using coarse powder. It seems that utilizing the coarse powder contributes to a better deposition efficiency as a 100 µm

NiCrAlY coating layer can be fabricated in 5 passes using the coarse powder and in 10 passes using the fine powder while the powder feed rate in both cases is 65 g/min. In addition, it was found that the grit-blasted 200 mesh sample has the best performance as a composite substrate as the coatings were deposited uniformly with high quality onto this type of substrate without damaging the substrate and peeling off the coated mesh cloth. However, some mesh cloth peeling off was observed once the 400 mesh substrate was used as the substrate. Another interesting observation is that the coating penetrates more into the mesh cloth and substrate when it is sprayed using the coarse powder. This might be explained by the fact that the coarse powder particles are notably heavier than the fine powder particles, and consequently, when they reach to the substrate, they have more momentum and penetrate more into the steel mesh cloth. It should also be noted that in all cases, the coatings did not reach and damage the composite fibers.

After analyzing the electrical properties of the coated samples, it was found that using the coarse NiCrAlY powder results in the formation of coatings with higher resistivity values, which is more useful for the fabrication of a heating element coating (will be discussed in detail in the next section). So, more composite substrates with bigger dimensions were coated with the coarse NiCrAlY powder for the electrical characterization and thermal analysis. The next two sections are more focused on the samples coated by the coarse powder.

3.4. Electrical Characterization

In this step, as mentioned in the previous chapter, the resistance of the coated samples was measured using the four-point probe method. The applied currents (6, 9, and 12 A) and the resultant voltages along the surface of the coatings, as well as other electrical properties (including resistance, resistivity, sheet resistance, and intensity), are shown in Table 3.2 for each type of coated samples. Figure 3.16 shows the V-I graphs for different coated samples. As expected, in all the cases, the voltage has a linear relationship with the current and given that$R = \frac{V}{I} = \frac{\Delta V}{\Delta I}$, the V-I curves slope represents the resistance of the coatings. From Figure 3.16, it is apparent that the sample coated in 3 passes has a higher value of resistance than the ones coated in 4 and 5 passes. In fact, as $R = \rho \frac{l}{A} = \rho \frac{l}{bd}$, the resistance is directly proportional to the electrical resistivity and length and inversely proportional to the cross-section area or, in other

words, to the cross-section thickness and width. So, by increasing the number of passes and consequently, the coating thickness, the resistance decreases. Another interesting observation is that when the number of coating passes decreases from 4 to 3, the resistance increases about 128% (from 0.07 to 0.158 Ω), while by decreasing the number of passes from 5 to 4, the resistance increases just about 13.5% (from 0.06 to 0.07 Ω). A possible explanation for these results is that the coating thickness does not increase with the number of passes linearly. By referring to the Figure 3.13-Figure 3.15, it can be seen that the coating sprayed in three passes is non-uniform and has a low average thickness, however, increasing the number of passes to 4, increases the coating thickness and uniformity, and results in lowering the resistance value considerably.

The resistance of the coated samples was also measured at different temperatures (25 to 150 ^{o}C). It was found that in that range of temperature, in all the cases, the resistance of the NiCrAlY coating is almost constant and independent of the coating surface temperature. After finding the resistance of the coated samples, the resistivity of the coatings was calculated using $\rho = R\frac{A}{l} = R\frac{bd}{l}$ equation. Resistivity is an intrinsic property that unlike resistance, does not depend on the shape and dimensions of the material. So, the resistivity value of two coatings sprayed with the same spray parameters but with the different number of passes should be similar and close to each other. However, as the spray parameter and powder size have a direct impact on the percentage of coating oxidation and porosity, changing them may result in different resistivity values. In addition, since the coatings are always associated with porosity and oxidation, their intrinsic properties like electrical resistivity are usually different from the bulk and pure materials. After the electrical characterization tests, it was found that the type of steel mesh cloth (200 or 400 mesh count) does not make a sensible difference in the electrical properties of the coatings. That is why the results presented in Table 3.2, and Figure 3.16 and Figure 3.17 are true for both coated 200 and 400 mesh substrates, except the results of the coating deposited in 5 passes, as deposition of coating in 5 passes (using the coarse powder) was just possible in the case of using 200 mesh substrate.

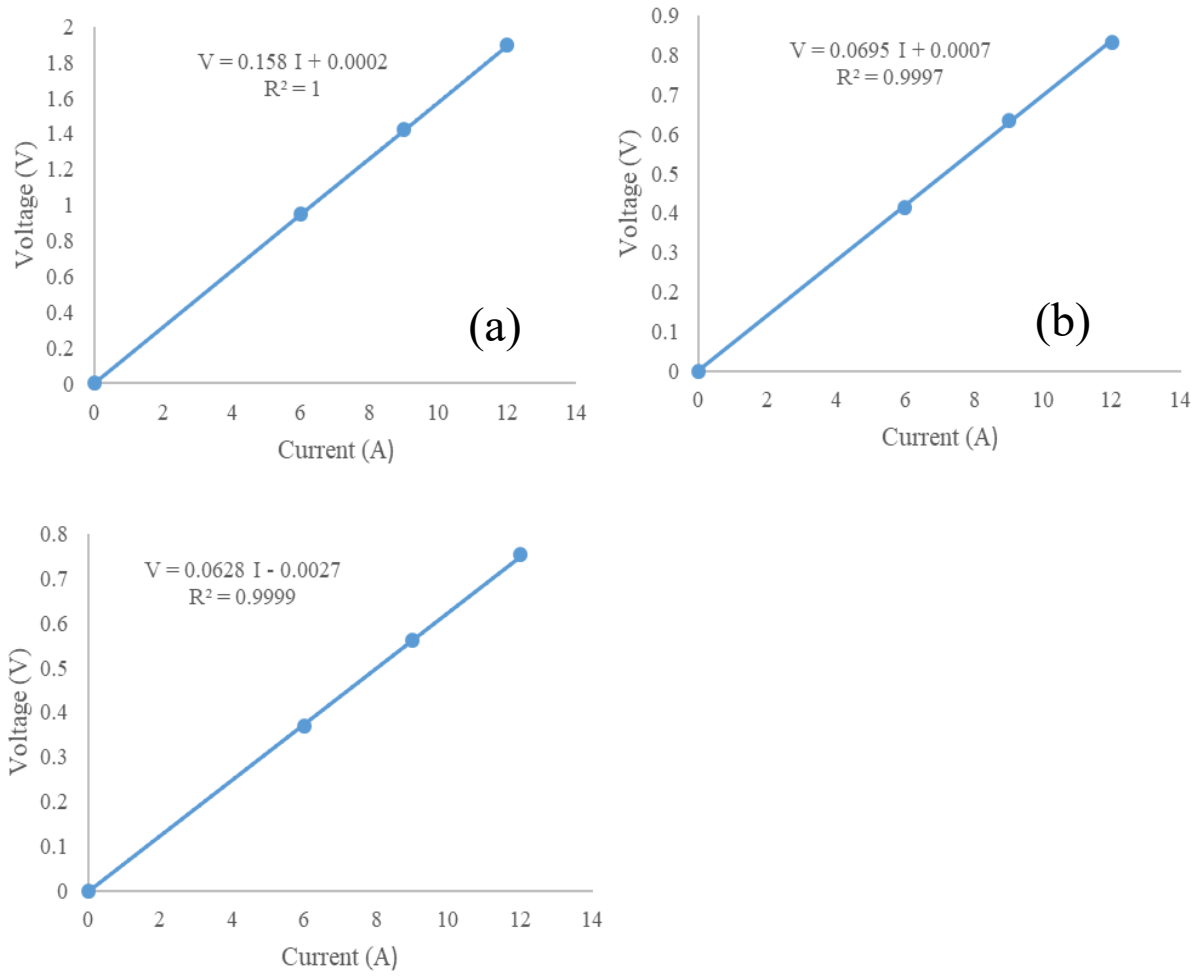

Figure 3.16: Voltage vs current for the NiCrAlY coatings deposited in, (a) 3 passes, (b) 4 passes, and (c) 5 passes.

As shown in Table 3.2, the resistivity values for the coatings sprayed in 4 and 5 passes using the coarse powder are very close and in the range of 2.2×10^{-6} to $2.30 \times 10^{-6}\Omega$.m. However, the resistivity of the coating sprayed using the fine powder is about $1.98 \times 10^{-6}\Omega$.m and approximately 14% lower than that of the coating sprayed using the coarse powder. In fact, using the coarse powder as the coating material resulted in the formation of a coating with higher resistivity. It is also worth noting that in all coatings, the resistivity is considerably higher in comparison to the bulk Nickel-Chromium alloys, in which the average resistivity value is about $1.6 \times 10^{-6}\Omega$.m, for two different reasons. In the coatings sprayed using fine powder, as shown in Figure 3.10e and g, although the porosity is low and the voids are small, the high oxidation

percentage contributed to increasing the resistivity value. On the contrary, as shown in Figure 3.14 and Figure 3.15, in the other type of coating (deposited using the coarse powder), the oxidation is relatively low and limited, but the high porosity and the presence of big void did lead to increasing the resistivity significantly. By comparing the resistivity values of the coated samples, it can be found that the presence of porosity and large voids play a more important role, in comparison to oxidation, in increasing the coating resistivity.

After finding electrical resistivity of the coatings, the sheet resistance was calculated using $R_S = \frac{\rho}{d}$ equation. Sheet resistance is, in fact, the resistance of a square sheet irrespective to its dimension, and is used more for the thin films and coatings. The most important advantage of sheet resistance over electrical resistance is its independency from the square size, which makes the comparison between different samples easy. It also shows the capability of a sample in generating heat when a given current is applied to it. As depicted in Table 3.2, the highest sheet resistance belongs to the sample coated in 3 passes using the coarse powder (about 0.058 Ω/□), and the lowest sheet resistance is for the sample coated by the fine powder (about 0.021 Ω/□). It means that the former coating generates more power and heat, compared to the other coated samples, for a given current. The sheet resistance values of the coatings sprayed in 4 and 5 passes are close to each other as their electrical resistivity is similar, and there is just an about 15% difference between their thicknesses.

Table 3.2: Electrical properties of the coated samples.

Number of coating passes	Powder type	current (A)	Voltage (V)	R (Ω)	Length (cm)	Width (cm)	Average thickness (μm)	ρ (μΩ.m)	Average ρ (μΩ.m)	Average sheet resistance (Ω/□)	Intensity (kW/m^2)
5	Coarse	6	0.368	0.0613	6	2.3	96±4.0	2.267	2.295±0.095	0.0239± 0.0020	1.599
		9	0.561	0.0623				2.301			3.658
		12	0.753	0.0627				2.316			6.547
4	Coarse	6	0.415	0.0691	6	2.3	83.5±4.2	2.150	2.170±0.109	0.0268± 0.0021	1.804
		9	0.635	0.0705				2.210			4.140
		12	0.83	0.0691				2.150			7.216
3	Coarse	6	0.949	0.1581	6	2.3	39±3.1	2.260	2.264±0.179	0.0580± 0.0100	4.312
		9	1.419	0.1576				2.260			9.673
		12	1.896	0.1580				2.260			17.236
10	Fine	6	0.127	0.0211	2.3	2.3	94±2.3	1.987	1.993±0.048	0.0212± 0.0020	1.438
		9	0.195	0.0216				2.033			3.310
		12	0.250	0.0208				1.960			5.676

3.5. Thermal Analysis

As pointed out in the previous chapter, once the electrical characterization was completed, the coated samples surface temperature was tested using thermocouples and infrared camera while they were connected to a power supply. In each set of experiments, three different currents (i.e. 6,9, and 12 A) were applied to the coated samples. The resultingvoltage, and the generated power per unit area, which is called intensity, are presented for the different coatings in Table 3.2. It is apparent that in all the coatings, the intensity goes up by increasing the current as $Intensity = \frac{P}{A} = \frac{1}{A}RI^2$, and the resistivity of the coatings is relatively constant and does not change noticeably by temperature. Higher intensity can also be translated into higher surface temperatures. So, the highest range of temperature would be expected to belong to the sample coated in three passes as it generates higher intensity, compared to the other coated sample, for a given current.

The temperature profile of the sample coated in 3 passes is illustrated in Figure 3.17. It is clear that the 12 and 6 A curves have the highest and lowest range of surface temperatures, respectively. From the 12 A curve, it can be seen that the curve slope, especially in the beginning, is very sharp, and the surface temperature goes up very quickly by time. The surface temperature reaches 100 °C in just 20 s, and it goes over 200 °C in about 90 s. It can also be seen that the 12 A curve has not reached steady-state during the test period. In fact, the sample was disconnected from the power supply once the surface temperature exceeded 200 °C as the glass-transient and curing temperature of the utilized composite material are about 90 and 120 °C, respectively, and keeping the sample above these temperatures for a long time may damage and burn the composite part. From the 9 A curve, it is apparent that the curve slope is smoother and the temperature increases slower over time in comparison to the 12 A curve. In this case, the surface temperature increases to 100 °C in about 45 s, and it reaches steady-state, in which the temperature is approximately 195 °C, in about 220 s. Finally, in the 6 A curve, the time that takes for reaching the temperature of 100 °C is about 135 s. The temperature also becomes steady-state (145 °C) in about 450 s. In fact, in this case, the temperature profile, especially after 150 s, has a very smooth slope, and the time that takes for reaching to the temperature of 100 °C or steady-state is considerably higher compared to the previous ones. By referring to Table 3.2, it can be seen that the intensity of a coated sample, connected to a 12 A power source, is about 2

and 4 times of those of samples connected to 9 and 6 A power sources, respectively. That is why the sample with the applied 12 A current always has a higher temperature and reaches a specific temperature notably earlier.

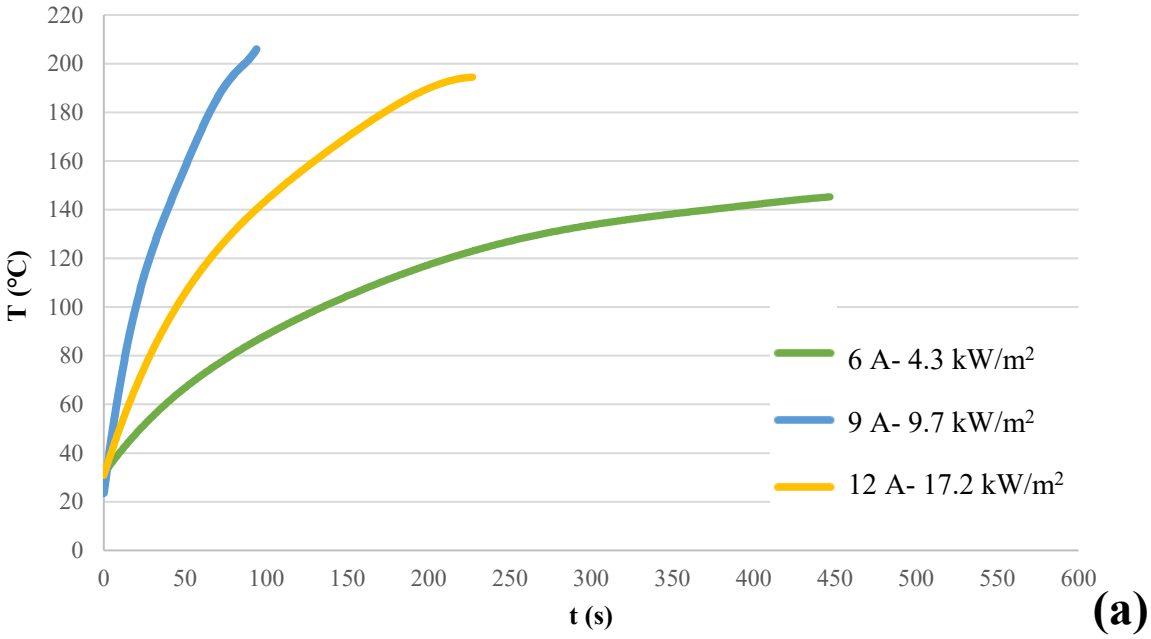

(a)

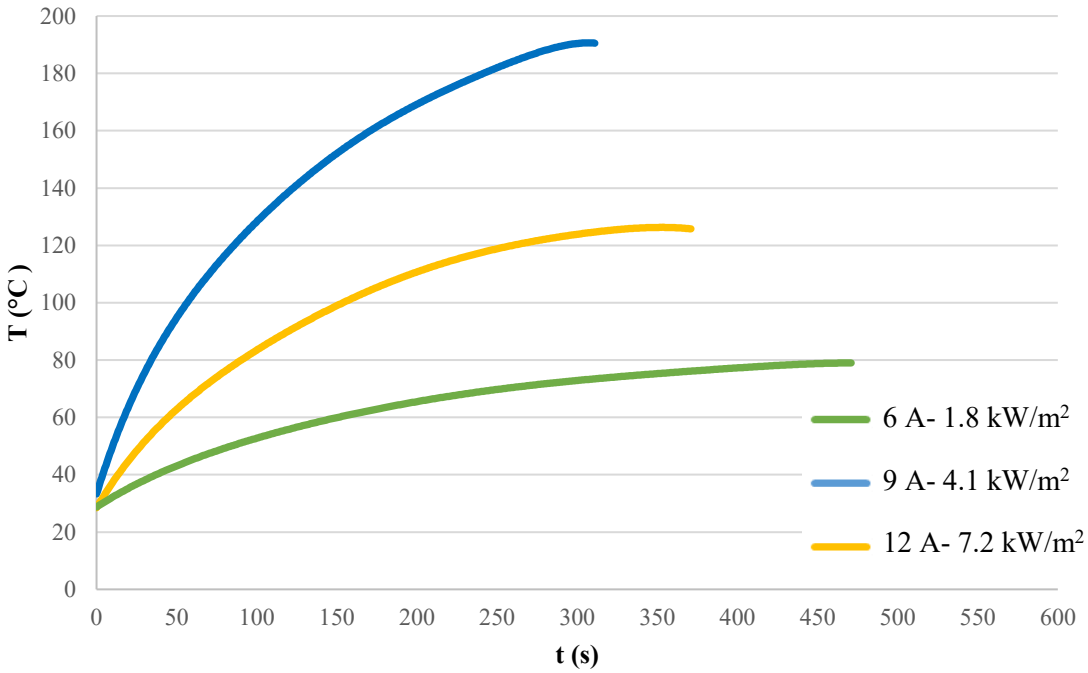

(b)

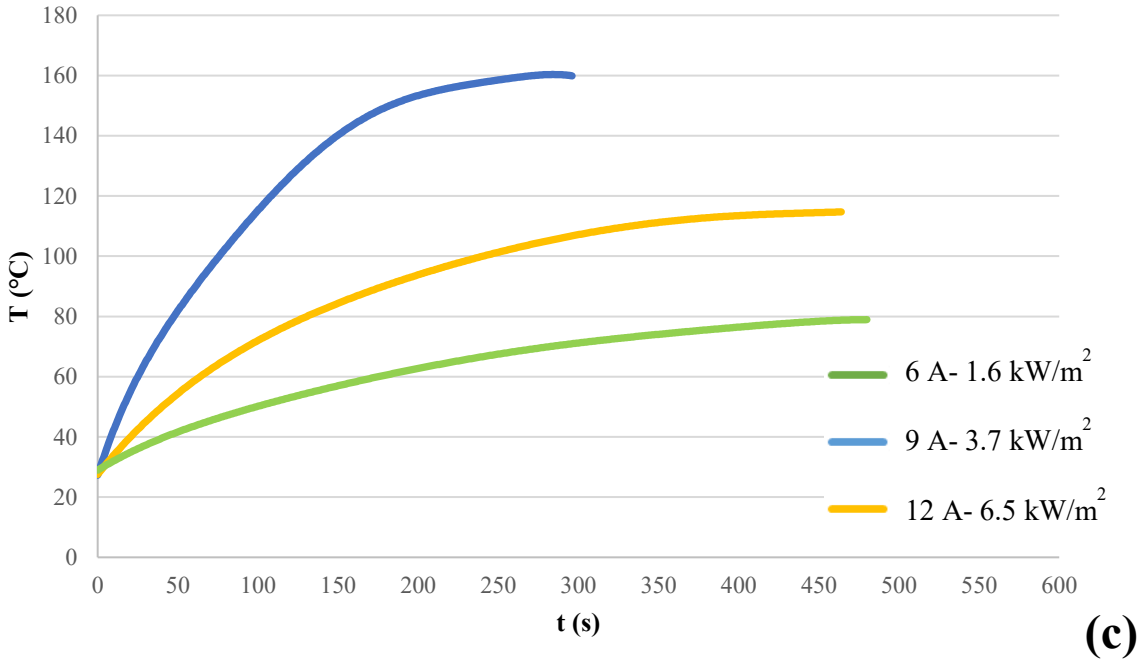

Figure 3.17: Average surface temperature vs time graphs of the coatings deposited in, (a) 3, (b) 4, and (c) 5 passes.

Figure 3.17b depicts the temperature profile of the sample coated in 4 passes whilst 6, 9, and 12 A currents were applied to it. It is apparent that the temperature trend in this case also is similar to that of the previous coating. By applying a 12 A current, the surface temperature increased to 100 °C in 55 s, and got steady-state (T=190 °C) after about 300 s. Applying a 12 A current also resulted in increasing the surface temperature to 100 °C in about 155 s, and reaching to steady state after 370 s. Finally, by connecting the coated sample to a 6 A current source, the temperature increases to 86 °C in 470 s (steady-state) and remained constant after that. By comparing Figure 3.17 a and b, it can be found that higher temperatures were achieved by using the sample coated in 3 passes. In addition, the amount of time needed for approaching a specific temperature or steady-state condition, especially in the cases of 12 and 9 A current, is considerably higher in the latter sample. It is due to the fact that the generated intensity of the 39 µm coating (deposited in 3 passes) is about twice the intensity of the 83.5 µm coating (deposited in 4 passes) for a given current. It can also be observed that the temperature profile and the performance of the 39 µm with an applied current of 9 A are similar to those of the 83.5 µm

coating with an applied current of 12 A as their intensity values are close to each other (see Table 3.2).

Figure 3.17c illustrates the temperature profile of the sample coated in 5 passes (96 µm coatings) after applying 6, 9, and 12 A currents. The range of temperature in this case is lower than the two previous coatings due to lower resistance, and consequently, the generation of lower intensity for a given current. However, the trend, shape, and relation of the curves with each other are very similar to the previous ones. By applying 12 A current, the surface temperature reached to 100 °C in 76 s, and to steady state (T=160 °C) in about 300 s. It can also be seen from the graph that once a 9 A current was applied to the coating, the temperature raised to 100 °C in 250 s, and got steady-state after about 460 s. Finally, when the coated sample was connected to the 6 A current source, the temperature increased to the steady-state temperature after 480 s.

It seems that the 39 µm coating has a better performance as a heating element due to the generation of more intensity, considerably higher surface temperature, and lower steady-state time. However, the surface temperature distribution results from this coating while it is connected to a power source is non-uniform. On the contrary, as shown in Figure 3.18, the surface temperature distributions that result from using 83 and 96 µm coatings as a heating element are very uniform. As mentioned earlier, the reason is that the 40 µm coating has a low uniformity (see Figure 3.13), and consequently the power generated in each part of the coating is not same, while in the two other cases, the coating has a high uniformity and the amount of generated power in the different parts of the coating is same. It should also be noted that in all these cases different constant currents were applied to the samples (i.e. 6, 9, and 12 A), however, if instead of applying constant currents, constant voltages be applied to the coated samples, the power (or intensity) generated using the 96 µm coating is notably higher than the other coatings as $P = \frac{V^2}{R}$, and the 96 µm coating has the lowest R value. So, based on the several factor like the application of heating element, where it is used, the amount of needed power, uniformity level of importance, and other limitation, each of these heating element coatings might be useful. Based on the literatures, the amount of intensity needed to be provided by the heating elements for de-icing purposes in Boeing 787 is in the range of 2.1-3.6 kW/m^2 (1.35-2.33 w/in^2) [11, 58, 59].

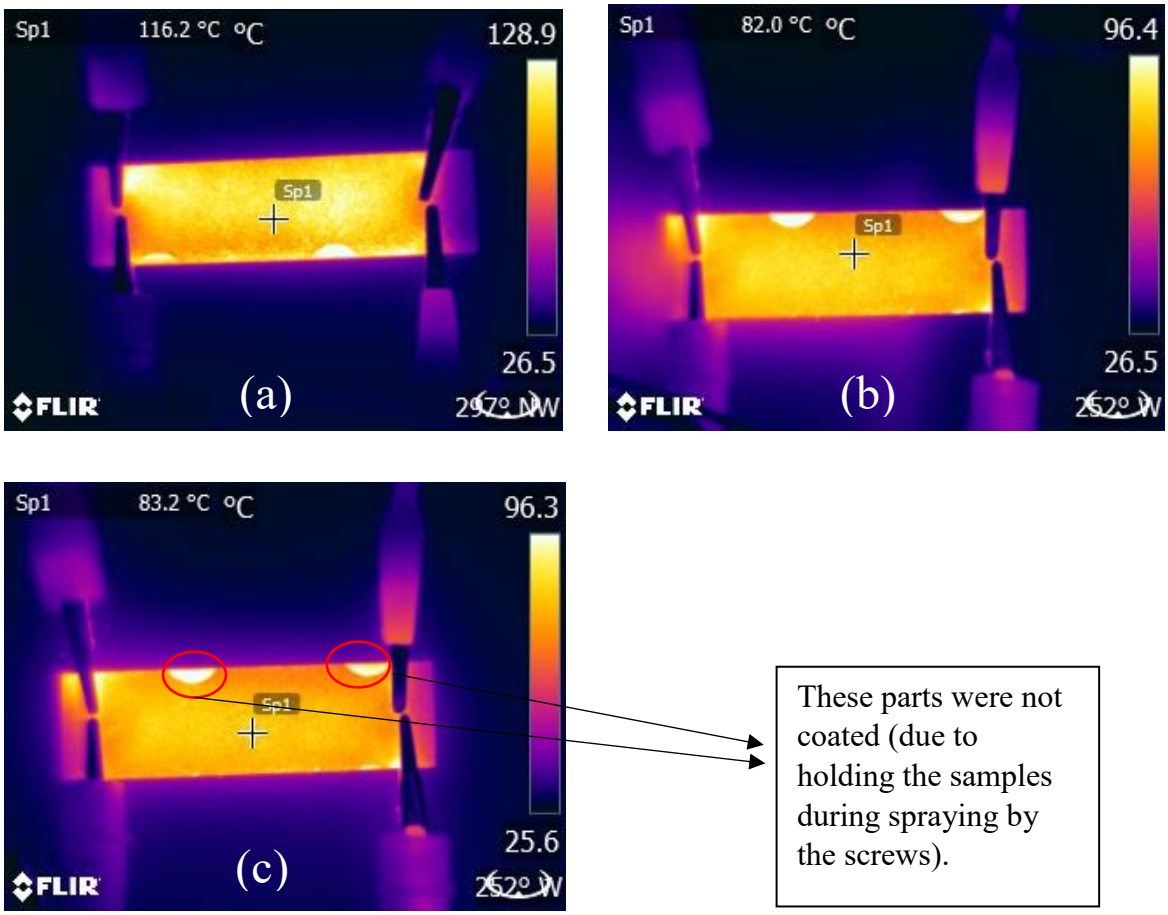

Figure 3.18: surface temperature of the composite samples coated by NiCrAlY in, (a) 3, (b) 4, and (c) 5 passes.

3.6. Adhesion Strength

The bonding strength results of the NiCrAlY coatings deposited onto the composite substrate are depicted in Figure 3.19. In this figure, the name of each sample is made of three parts. The first part specifies the type of coating material (*F* stands the fine powder and *C* stands for the coarse powder), the second part stands for the number of passes in which the coating was deposited in, and the third part specifies the type of composite substrate (*200* stands for the 200 mesh substrate and *400* stands for 400 mesh substrate). It should be noted to make sure about the reliability of the results, adhesion strength test was repeated 3 times for each coated sample. As shown in Figure 3.19, samples C-4-200 and F-10-200 have the highest coating adhesion strength. Another interesting observation is that globally the samples in which 200 mesh composites were

used as the substrate (except C-5-200) have a higher adhesion strength compared to the samples in which 400 mesh composites were used as the substrate. In all coated 400 mesh substrates (C-3-400 and C-4-400), the failure occurred during the adhesion test at the interface of the steel mesh cloth and the composite part (see Figure 3.20). This is due to the imperfect bonding of the 400 mesh cloth to the composite part (see Figure 3.2). So, this might be concluded that the maximum adhesion strength in the case of a coated 400 mesh substrate is around 15 MPa as in the higher tensions the steel mesh cloth detach from the substrate. On the other hand, as shown in Figure 3.20, the failure mode in the cases in which 200 mesh composites were used as the substrate, is a combination of coating failure and mesh cloth failure. The lowest bonding strength was achieved for sample C-5-200. This observed decrease in the adhesion strength could be attributed to the significant stresses that were induced to the substrate due to increasing the number of passes and coating thickness, as well as being in the exposure of hot gas temperatures for a longer amount of time. The adhesion strength values obtained for sample C-4-200 and F-10-200 are about 50% higher than the adhesion strength values reported for the coated composites in the literature [2, 20].

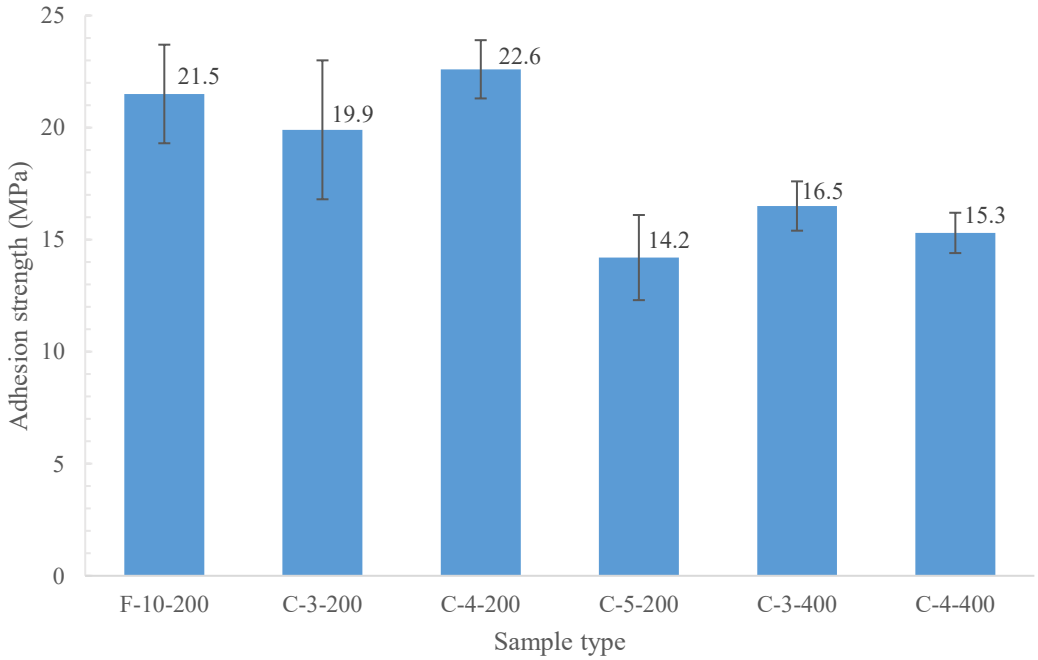

Figure 3.19: Adhesion strength results of the coated samples.

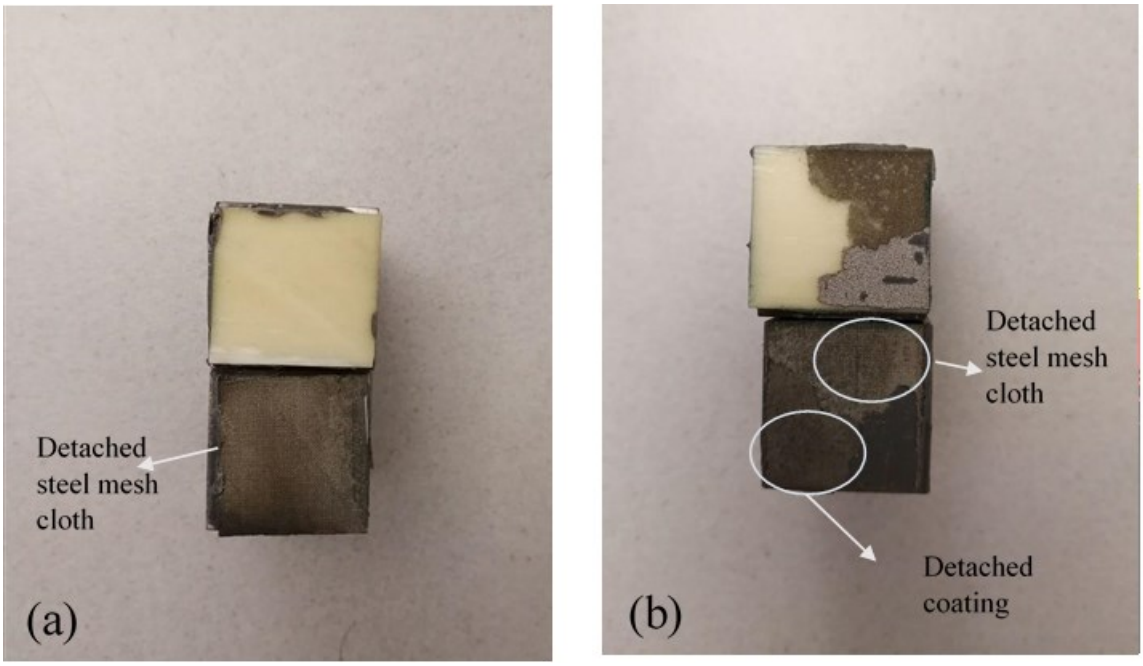

Figure 3.20: Failure mode in the coated samples in which, (a) 400 mesh composite, and (b) 200 mesh composites were used as the substrate.

Chapter 4: Conclusion & Future Work

4. Conclusion and Future Work

4.1. Conclusion

In present study, the fabrication of a NiCrAlY coating layer on polymer-based composite materials for the de-icing application using the plasma spray technique was investigated. The main purpose of the current investigation was to deposit a uniform and high-quality NiCrAlY coating layer on the top of a GFRP sample without damaging and burning the composite part.

Due to the fact that impact of high-velocity particles induce significant damages to the composite materials, especially fibers, using common preparation methods (prior to the coating process) like grit blasting without proper surface modification is not possible. In addition, polymeric materials usually have low service temperature while in a thermal spray process like plasma spraying, the flame temperature may even reach 12000 °C. Therefore, using an appropriate cooling system for managing the temperature of the composite substrates during spraying is crucial. The low free surface energy and high chemical inertness of the polymeric materials also makes the deposition of a metallic coating layer very difficult.

In this study, three types of composite substrates were made by using glass fiber-reinforced polymer prepreg plies (GFRP) and stainless steel mesh cloth, which are: 1) typical composite substrate, 2) 200 mesh substrate which was made by incorporation of an extra 200 stainless steel mesh cloth on top of the prepregs during the fabrication process, and 3) 400 mesh substrate which was made by incorporation of an extra 400 stainless steel mesh cloth on top of the prepregs during the fabrication process. After preparing the composite substrates by grit blasting, the samples were coated by fine and coarse NiCrAlY powders.

The microscopic images of the coated sample cross-sections revealed that the deposition of the metallic coating onto typical composites is very limited. In this case, the grit blasting also resulted in breaking and damaging the composite fibers significantly. However, in the cases of 200 and 400 mesh substrates, it was observed that a uniform NiCrAlY coating with high deposition efficiency and uniformity could be deposited by using a proper set of spray parameters. Indeed, the incorporation of the stainless steel mesh cloths to the composite structure not only did increase the surface free energy and improve the coating adhesion but also played the role of armor for the composite part and protected the composite fibers from the impact of

high-velocity particles during grit blasting and spraying. It was also observed that the 400 mesh substrates, especially in the relatively harsh spray conditions, are more susceptible to the steel mesh cloth peeling off during spraying due to its weak and thin steel wires, as well as the imperfect bonding existing between the cloth and composite part. The microscopic images also showed that the coatings generated by the fine powder have more uniformity and lower porosity compared to the coatings generated by the coarse powder.

All the coated samples showed a high capability in generating heat and acting as a heating element. The results of the electrical characterization of the coated samples also indicated that using NiCrAlY powder with the coarse size distribution (compared to the fine powder) results in the formation of coatings with higher resistivity and sheet resistance. Using this type of coating also contributed to the generation of more intensity (power per unit area) for a given current. As utilizing the coarse powder resulted in higher resistivity value and higher deposition efficiency during spraying, more composite samples with larger dimensions were coated using this powder in 3, 4, and 5 passes, which contributed to the creation of coatings with thicknesses of 39, 83, and 96 μm, respectively. The resistance of 39 μm coating was considerably higher than that of 83 and 96 μm coatings. The intensity generated using this coating was also notably higher for a given current. However, the disadvantage of using this 39 μm coating as a heating element is its non-uniform cross-section, which results in the formation of a non-uniform surface temperature distribution once it is connected to a power supply. On the contrary, the coatings deposited in 4 and 5 passes had a relatively uniform cross-section and surface temperature distribution. Depends on the application and limitations, each of these coated samples might be useful as a heating element.

Finally, the results of the coating adhesion test revealed that in many cases, the coatings have a bonding strength, even about 50% more than something reported in the literature [2, 20]. The results also showed that the coating bonding strength in the cases in which the 200 mesh composite was used as the substrate was considerably higher compared to those coated samples in which 400 mesh composite was used as the substrate. It was also observed that in the coated 400 mesh substrates, the detachment occur in the interface steel mesh cloth and the composite. It was also found when the coarse NiCrAlY is used as the coating material, increasing the number of passes from 4 to 5 leads to a significant decrease in the coating adhesion strength.

4.2. Future Work

The findings achieved in this study suggest the following directions for future research:

- Investigating the performance of using stainless steel mesh cloth on improving the coating deposition efficiency and adhesion of other types of coatings on polymeric materials.

- Using other metallic materials instead of NiCrAlY like NiCr, FeCrAl, and FeCrAlY for the deposition of a heating element coating onto the composite structures, and comparing their performances with each other.

- Using other preparation methods like chemical treatment for preparing the composite substrates before the coating deposition process.

- Using different metallic mesh cloths with different materials and different mesh counts for improving the coating adhesion strength.

- Analyzing the impacts of composite properties (e.g. composites glass transition and curing temperatures) on the coating adhesion.

- Investigating the other applications of a NiCrAlY-coated GFRP composite.

References

References

[1] G. Sun, X. He, J. Jiang, Y. Sun, and Y. Zhong, "A study on the deposition of Al 2 O 3 coatings on polymer substrates by a plasma spray/micro-arc oxidation two-step method," *Journal of thermal spray technology,* vol. 22, no. 1, pp. 27-35, 2013.

[2] A. Liu, M. Guo, J. Gao, and M. Zhao, "Influence of bond coat on shear adhesion strength of erosion and thermal resistant coating for carbon fiber reinforced thermosetting polyimide," *Surface and Coatings Technology,* vol. 201, no. 6, pp. 2696-2700, 2006.

[3] W. Huang *et al.*, "Effect of bond coats on thermal shock resistance of thermal barrier coatings deposited onto polymer matrix composites via air plasma spray process," *Journal of Thermal Spray Technology,* vol. 22, no. 6, pp. 918-925, 2013.

[4] Z. Goraj, "An overview of the de-icing and anti-icing technologies with prospects for the future," in *24th international congress of the aeronautical sciences*, 2004, vol. 29.

[5] M. Sinnett, "787 no-bleed systems: saving fuel and enhancing operational efficiencies," *Aero Quarterly,* vol. 18, pp. 6-11, 2007.

[6] M. Davies, *The standard handbook for aeronautical and astronautical engineers*. McGraw-Hill, 2003.

[7] E. Jr. "Aircraft anti icing & de-icing sytems." https://www.slideshare.net/ErangaJrABW/aircraft-anti-icing-de-icing-sytems-project-report (accessed April 24, 2019).

[8] M. E. McMann. "TKS Ice Protection." https://www.planeandpilotmag.com/article/tks-ice-protection/#.XTlCdOhKhPZ (accessed 25 April, 2019).

[9] K. Al-Khalil, "Thermo-Mechanical Expulsive De-icing System-TMEDS," in *45th AIAA aerospace sciences meeting and exhibit*, 2007, p. 692.

[10] "Low Power Ice Protection Systems." Cox & Company. http://www.coxandco.com/low_power_ips.html (accessed April 24, 2019).

[11] J. Sloan, "787 integrates new composite wing de-icing system," *High Performance Composites,* vol. 17, no. 1, pp. 27-29, 2009.

[12] L. K. Phillips, "Drinking water dispensing system for automobiles and associated method," ed: US Patents, 2012.

[13] P. L. Fauchais, J. V. Heberlein, and M. I. Boulos, *Thermal spray fundamentals: from powder to part*. Springer Science & Business Media, 2014.

[14] J. R. Davis, *Handbook of thermal spray technology*. ASM international, 2004.

[15] L. Pawlowski, *The science and engineering of thermal spray coatings*. John Wiley & Sons, 2008.

[16] M. Oksa, E. Turunen, T. Suhonen, T. Varis, and S.-P. Hannula, "Optimization and characterization of high velocity oxy-fuel sprayed coatings: techniques, materials, and applications," *Coatings,* vol. 1, no. 1, pp. 17-52, 2011.

[17] J. Flock, K. Friedrich, and Q. Yuan, "On the friction and wear behaviour of PAN- and pitch-carbon fiber reinforced PEEK composites," *Wear,* vol. 225, pp. 304-311, 1999.

[18] A. Liu, M. Guo, M. Zhao, H. Ma, and S. Hu, "Arc sprayed erosion-resistant coating for carbon fiber reinforced polymer matrix composite substrates," *Surface and Coatings Technology,* vol. 200, no. 9, pp. 3073-3077, 2006.

[19] S. Guanhong, H. Xiaodong, J. Jiuxing, and S. Yue, "Parametric study of Al and Al2O3 ceramic coatings deposited by air plasma spray onto polymer substrate," *Applied Surface Science,* vol. 257, no. 17, pp. 7864-7870, 2011.

[20] A. Ganesan, M. Yamada, and M. Fukumoto, "The effect of CFRP surface treatment on the splat morphology and coating adhesion strength," *Journal of Thermal Spray Technology,* vol. 23, no. 1-2, pp. 236-244, 2014.

[21] R. Lima *et al.*, Agarwal, A., Hyland, M.M., Lau, Y.C., Li, C.J., McDonald, A. and Toma, F.L "Temperature Measurements of Polymer Composite Flat Plates Coated with Aluminum-12Silicon," 2012.

[22] R. Gonzalez, A. McDonald, and P. Mertiny, "Effect of flame-sprayed Al–12Si coatings on the failure behaviour of pressurized fibre-reinforced composite tubes," *Polymer Testing,* vol. 32, no. 8, pp. 1522-1528, 2013.

[23] D. S. Therrien, "Heat Transfer Analysis of Flame-sprayed Metal-polymer Composite Structures," 2013.

[24] H. Ashrafizadeh, A. McDonald, and P. Mertiny, "Deposition of electrically conductive coatings on castable polyurethane elastomers by the flame spraying process," *Journal of Thermal Spray Technology,* vol. 25, no. 3, pp. 419-430, 2016.

[25] A. Ganesan, M. Yamada, and M. Fukumoto, "Cold spray coating deposition mechanism on the thermoplastic and thermosetting polymer substrates," *Journal of Thermal Spray Technology,* vol. 22, no. 8, pp. 1275-1282, 2013.

[26] A. Sturgeon, B. Dunn, S. Celotto, and W. O'Neill, "Cold sprayed coatings for polymer composite substrate," *ESA SP,* vol. 616, no. 1, pp. 1-5, 2006.

[27] R. Gonzalez, A. McDonald, and P. Mertiny, "Damage detection method for fiber-reinforced polymer composites using Al-12Si flame-sprayed coatings," in *Society of Advancement of Material and Process Engineering (SAMPE) 2014 Conference*, 2014, pp. 2-5.

[28] A. Lopera-Valle and A. McDonald, "Application of flame-sprayed coatings as heating elements for polymer-based composite structures," *Journal of Thermal Spray Technology,* vol. 24, no. 7, pp. 1289-1301, 2015.

[29] A. Lopera-Valle and A. McDonald, "Flame-sprayed coatings as de-icing elements for fiber-reinforced polymer composite structures: Modeling and experimentation," *International Journal of Heat and Mass Transfer,* vol. 97, pp. 56-65, 2016.

[30] K. E. Schneider, V. Belashchenko, M. Dratwinski, S. Siegmann, and A. Zagorski, *Thermal spraying for power generation components*. John Wiley & Sons, 2006.

[31] R. Gonzalez, H. Ashrafizadeh, A. Lopera, P. Mertiny, and A. McDonald, "A review of thermal spray metallization of polymer-based structures," *Journal of Thermal Spray Technology,* vol. 25, no. 5, pp. 897-919, 2016.

[32] F. Gärtner, T. Stoltenhoff, T. Schmidt, and H. Kreye, "The cold spray process and its potential for industrial applications," *Journal of Thermal Spray Technology,* vol. 15, no. 2, pp. 223-232, 2006.

[33] V. K. Champagne, D. Helfritch, P. Leyman, S. Grendahl, and B. Klotz, "Interface material mixing formed by the deposition of copper on aluminum by means of the cold spray process," *Journal of Thermal Spray Technology,* vol. 14, no. 3, pp. 330-334, 2005.

[34] X. Zhou, A. Chen, J. Liu, X. Wu, and J. Zhang, "Preparation of metallic coatings on polymer matrix composites by cold spray," *Surface and Coatings Technology,* vol. 206, no. 1, pp. 132-136, 2011.

[35] A. Ganesan, J. Affi, M. Yamada, and M. Fukumoto, "Bonding behavior studies of cold sprayed copper coating on the PVC polymer substrate," *Surface and Coatings Technology,* vol. 207, pp. 262-269, 2012.

[36] H. Ye and J. Wang, "Preparation of aluminum coating on Lexan by cold spray," *Materials Letters,* vol. 137, pp. 21-24, 2014.

[37] P. C. King, A. J. Poole, S. Horne, R. de Nys, S. Gulizia, and M. Z. Jahedi, "Embedment of copper particles into polymers by cold spray," *Surface and Coatings Technology,* vol. 216, pp. 60-67, 2013, doi: 10.1016/j.surfcoat.2012.11.023.

[38] M. Gardon, A. Latorre, M. Torrell, S. Dosta, J. Fernández, and J. Guilemany, "Cold gas spray titanium coatings onto a biocompatible polymer," *Materials Letters,* vol. 106, pp. 97-99, 2013.

[39] A. Moridi, S. M. Hassani-Gangaraj, M. Guagliano, and M. Dao, "Cold spray coating: review of material systems and future perspectives," *Surface Engineering,* vol. 30, no. 6, pp. 369-395, 2014.

[40] R. Lupoi and W. O'Neill, "Deposition of metallic coatings on polymer surfaces using cold spray," *Surface and Coatings Technology,* vol. 205, no. 7, pp. 2167-2173, 2010.

[41] M. Fukumoto, H. Terada, M. Mashiko, K. Sato, M. Yamada, and E. Yamaguchi, "Deposition of copper fine particle by cold spray process," *Materials Transactions,* pp. 0904200749-0904200749, 2009.

[42] M. J. Vucko, P. C. King, A. J. Poole, C. Carl, M. Z. Jahedi, and R. de Nys, "Cold spray metal embedment: an innovative antifouling technology," *Biofouling,* vol. 28, no. 3, pp. 239-248, 2012.

[43] M. Ivosevic, R. Knight, S. R. Kalidindi, G. R. Palmese, and J. K. Sutter, "Adhesive/cohesive properties of thermally sprayed functionally graded coatings for polymer matrix composites," *Journal of Thermal Spray Technology,* vol. 14, no. 1, pp. 45-51, 2005.

[44] M. Ivosevic, R. Knight, S. Kalidindi, G. Palmese, and J. Sutter, "Solid particle erosion resistance of thermally sprayed functionally graded coatings for polymer matrix composites," *Surface and Coatings Technology,* vol. 200, no. 16-17, pp. 5145-5151, 2006.

[45] W. Huang *et al.*, "Fabrication of thermal barrier coatings onto polyimide matrix composites via air plasma spray process," *Surface and Coatings Technology,* vol. 207, pp. 421-429, 2012.

[46] J. Affi, H. Okazaki, M. Yamada, and M. Fukumoto, "Fabrication of aluminum coating onto CFRP substrate by cold spray," *Materials Transactions,* pp. 1108081451-1108081451, 2011.

[47] S. V. Hoa, *Principles of the manufacturing of composite materials*. DEStech Publications, Inc, 2009.

[48] "Woven Wire Mesh." https://www.inoxia.co.uk/products/mesh/sheets/ (accessed May 10, 2019).

[49] "Vacuum Bagging Equipment and Techniques for Room-Temp Applications." https://www.fibreglast.com/product/vacuum-bagging-equipment-and-techniques-for-room-temp-applications/Learning_Center (accessed April 10, 2019).

[50] "Cytec-CYCOM E773." https://www.e-aircraftsupply.com/products/Resin/48829/CYCOM-E-773 (accessed March 26, 2019).

[51] "MCrAlY Alloy Powder Materials for Thermal Spray." https://www.oerlikon.com/metco/en/products-services/coating-materials/coating-materials-thermal-spray/mcraly-alloys/ (accessed May 17, 2019).

[52] "3MB Plasma Spray Gun - Oerlikon Metco." https://www.oerlikon.com/metco/en/products-services/coating-equipment/thermal-spray/spray-guns/coating-equipment-plasma/3mb/ (accessed July 18, 2019).

[53] "Resistance and Resistors-Ohm's Law." https://courses.lumenlearning.com/boundless-physics/chapter/resistance-and-resistors/ (accessed July 20, 2019).

[54] V. Msomi, "Vanadium dioxide thermochromic thin films correlation between microstructure, electrical and optical properties," Citeseer, 2008.

[55] "Surface Energy Chart." http://www.technibond.co.uk/Portals/0/blog-img/surface-energy-chart.pdf (accessed March 3, 2019).

[56] "How To Prepare Surfaces For Thermal Spray Coatings | A&A Thermal Spray Coatings." https://www.thermalspray.com/how-to-prepare-surfaces-for-thermal-spray-coatings/ (accessed March 19, 2019).

[57] D. Seo and K. Ogawa, "Isothermal oxidation behavior of plasma sprayed MCrAlY coatings," *Advanced Plasma Spray Applications,* pp. 61-82, 2012.

[58] A. Shinkafi, C. Lawson, R. Seresinhe, D. Quaglia, and I. Madani, "An Intelligent Ice Protection System for Next Generation Aircraft Trajectory Optimisation," *St. Petersburgh, Russia,* 2014.

[59] O. Meier and D. Scholz, "A handbook method for the estimation of power requirements for electrical de-icing systems," *DLRK, Hamburg*, vol. 31, 2010.